Thermal management of photovoltaics using phase change materials

MPF Verheijen

TU Delft

Thermal management of photovoltaics using phase change materials

by

M.P.F. Verheijen

to obtain the degree of Master of Science
at the Delft University of Technology,
to be defended publicly on Friday August 30, 2019 at 10:00 AM.

Student number:	1521934	
Project duration:	November 19, 2018 – August 30, 2019	
Thesis committee:	Dr. ir. Olindo Isabella,	TU Delft, supervisor
	Prof. Dr. Ir. Miro Zeman,	TU Delft
	Prof. Ir. Peter Luscuere,	TU Delft
	Ir. Juan Camilo Ortiz Lizcano,	TU Delft, daily supervisor

TU Delft

Abstract

While there are many factors influencing the efficiency of photovoltaic (PV) cells one of the most important ones is temperature. Module temperatures can get significantly higher than the ambient temperature, increases of up to $30°C$ have been reported in literature. An increase in temperature has an adverse effect on the module's efficiency, literature has reported a drop of $0.40 - 0.65\%/°C$. Therefore, it is not uncommon that during warm sunny days PV modules operate at a much lower efficiency than advertised by the manufacturer.

Different methods of thermal management can be applied. In this research, the effect of phase change materials (PCM) to passively lower the operating temperature of PV panels was studied. During the phase change of a material heat is absorbed as latent heat instead of sensible heat, this does not cause the temperature of the material to increase. Using this process a PCM can keep a relatively stable temperature until it has completely changed its phase. This can be utilised by placing PCM behind a PV module, so that the heat generated in the panel can be absorbed by the PCM while remaining at a stable temperature.

The scope of this research was to perform measurements with a PV-PCM system under real weather conditions. Additionaly, a thermal model was build using *Comsol Multiphysics*, to make predictions for the optimal PCM parameters. This thermal model was validated with the results from the measurements.

Measurements for a free rack situation showed surprisingly a slight increase in temperature of the PV-PCM module compared to a reference PV module. Most likely due to convective cooling caused by the wind. And indeed, after installing insulation material at the back of the modules to emulate building integrated photovoltaics (BIPV) a significant decrease was found. For a two week period of measuring a $-6.69°C$ temperature reduction was found, with a peak difference of $-21.7°C$. This resulted in an energy yield increase of 2.8% compared to the reference panel over this period.

From this work, it can be concluded that PCM thermal management is not advisable for free standing modules due to the large influence of convective cooling caused by the wind. However, this method of thermal management can have significant benefits in BIPV situations where convection is not relevant.

Acknowledgement

I would first like to thank my daily supervisor Ir. Juan Camilo Ortiz Lizcano. Whose office door was always open whenever I ran into a trouble spot or had a question about my research or writing. He consistently allowed this paper to be my own work, but steered me in the right the direction whenever he thought I needed it.

I would also like to thank our technician Stefaan Heirman without whom, the installation and measurements of the system would never have been possible.

I would also like to acknowledge the company OC Autarkis, for providing the PCM slabs which were the foundation of this research.

Finally, I must express my very profound gratitude to my parents and to my girlfriend Diána for providing me with unfailing support and continuous encouragement through the process of researching and writing this thesis. This accomplishment would not have been possible without them. Thank you.

M.P.F. Verheijen
Delft, August 2019

Contents

List of Figures ix

List of Tables xi

1 Introduction 1
1.1 Temperature dependence of photovoltaics . . . 1
1.2 Thermal management methods. . . . 1
1.2.1 Natural convection. . . . 2
1.2.2 Forced convection . . . 2
1.2.3 Water cooling . . . 2
1.2.4 Heat pipes . . . 2
1.2.5 Phase change materials . . . 2
1.3 Previous Work. . . . 2
1.4 Focus of this thesis . . . 3
1.5 Outline of this thesis . . . 3

2 Theory 5
2.1 Effects of temperature on a photovoltaic cell . . . 5
2.1.1 Series resistance . . . 5
2.1.2 Short circuit current . . . 6
2.1.3 Open circuit voltage . . . 6
2.2 Heat transfer . . . 7
2.2.1 Conduction . . . 7
2.2.2 Convection. . . . 7
2.2.3 Radiation . . . 8
2.2.4 Phase change . . . 8

3 Thermal Model and PCM parameters 11
3.1 Numerical method . . . 11
3.2 Geometry definition . . . 11
3.3 Material properties . . . 12
3.4 Heat Transfer Physics . . . 12
3.4.1 Convection. . . . 12
3.4.2 Radiation . . . 13
3.4.3 Weather data input. . . . 13
3.5 PCM properties . . . 13
3.6 Effect of varying PCM parameters. . . . 15
3.6.1 Latent Heat . . . 15
3.6.2 Thermal Conductivity . . . 16
3.6.3 PCM Thickness . . . 16
3.6.4 Melting Temperature. . . . 17

4 Experimental Setup 19
4.1 Module Design . . . 19
4.1.1 Coverage Factor . . . 19
4.1.2 Construction. . . . 20
4.2 Characterisation . . . 21
4.2.1 Module parameters . . . 22
4.2.2 Electroluminescence. . . . 23
4.3 Measurement . . . 23
4.3.1 Thermocouples . . . 23

5 Results, Validation & Predictions 25
5.1 Free standing rack . . . 25
5.1.1 Results measurement . . . 25
5.1.2 Validation . . . 26
5.1.3 Predictions . . . 27
5.1.4 Cold month . . . 29
5.2 Insulated backside . . . 29
5.2.1 Measurement results . . . 30
5.2.2 Validation . . . 30
5.2.3 Predictions . . . 31

6 Conclusions & Recommendations 35

A Effective temperature difference 37

B Plane of Array Irradiance 38

C Root mean square error 40

D Validation Data 41

Bibliography 45

List of Figures

1.1 Temperature difference between modules with and without PCM under a LASS taken from [29]. 3

2.1 The effect of an increased series resistance on the IV-curve [12]. 5
2.2 Effect of an increased temperature on the IV-curve of a solar cell. 7
2.3 Schematic figure of all heat transfer mechanisms within a PV panel. 7
2.4 Enthalpy of a phase change with and without hysteresis. 9

3.1 Cross-sectional model of a PV module with a PCM slab attached to the back, as it is used in the simulations (not to scale).*:Only added for PCM+T module. **:Added for the second set of simulations. 11
3.3 Melting temperature and melting enthalpy (latent heat) ranges of different types of PCM [22]. . 14
3.4 Two temperatures are taken: 1, the module temperature between the PV and PCM. 2, the back temperature behind the PCM. 15
3.5 The ambient temperature and irradiance during the summer day used for the simulations. . . . 15

4.1 Hindrance of PCM placement due to the junction box, causing significant temperature differences within the panel [29]. 19
4.2 Schematic of the panel layout using 5-inch IBC cells in a 4x4 grid, with a small junction box. . . 20
4.3 IBC cells connected in a single series string. 20
4.4 21
4.5 The junctionbox is super glued to the back of the panel, and sealed with silicone from both in and outside. 21
4.6 The modules are placed into an aluminium frame, which serves a dual purpose of allowing attachment to the rack and holding the PCM slabs in place. 22
4.7 Rooftop monitoring station rack with the three modules attached. 22
4.8 IV-curves for the different modules under the LASS. 23
4.9 Electroluminescence pictures of the three modules. 23
4.10 Illustration of the position of all the thermocouples at the back of the modules in red and the unmeasured cells in blue. 24
4.11 Temperature deviation of each thermocouple from the average temperature over all thermocouples. 24

5.1 Measured module temperatures from 2 July until 8 July. 26
5.2 Comparison of the measured and simulated data from 4-8 July. 27
5.3 The predicted module temperature for the simulation results of the PVGIS data of three situations that produce the best thermal performance. 28
5.4 The predicted module temperature for the simulation results of the PVPortal data of three situations that produce the best thermal performance. 28
5.5 The predicted module temperature for the simulation results of the measured data of three situations that produce the best thermal performance. 29
5.6 The predicted module temperature for several cold days in January using the predicted optimal parameters. 29
5.7 Measured module temperatures from 29 July until 2 August for all three modules. 30
5.8 Measured and simulated module temperature for the reference module for three days of the measuring period. 31
5.9 Measured and simulated module temperature for the PCM module for three days of the measuring period. 31
5.10 The predicted module temperature for the insulated simulation results of the PVGIS data of the situation with the best thermal performance. 32

5.11 The predicted module temperature for the insulated simulation results of the measured data of the situation with the best thermal performance. 33

B.1 Illustrating the angles used to describe the orientation of a PV module installed on a horizontal plane [9]. 38

D.1 Comparison of the measured and simulated data from 2-22 July. 42
D.2 Comparison of the measured and simulated data from 2-22 July for the PCM module. 43
D.3 Comparison of the measured and simulated data from 2-22 July for the PCM+T module. 44

List of Tables

1.1 Advantages and disadvantages of different thermal management techniques, adaptation from [6], [7], [8]. . . . 2

3.1 Material properties of the PV module used for the Comsol model. . . . 12
3.2 Different empirical convection models. . . . 13
3.3 Material properties of the PCM slabs used in both experimental and predictions. . . . 14

4.1 Parameters for all three modules as measured under the LASS. . . . 22

5.1 Energy yield and percentage wise improvement over the measured period from 2-22 July without insulation. . . . 26
5.2 Root mean square error values of different simulated models compared to measured values. . . . 27
5.3 Table with the top three PCM parameters for the PVGIS, PVPortal, and measured data. . . . 27
5.4 Energy yield and percentage wise improvement over the measured period from 26 July - 7 Aug with insulation. . . . 30
5.5 Table with the predicted best PCM parameters for the PVGIS and measured data. . . . 32

1
Introduction

Due to the growing global demand in energy and especially the demand for more sustainable solutions in energy production. Energy efficient design, and sustainable use of resources are increasingly required for the development of new technologies. Photovoltaics play a large role in providing a part of these sustainable solutions, as photovoltaic modules are easy to install and are becoming increasingly cost efficient due to the economy of scale. Prices being over $70 per Watt in the 1970s dropping to under $1.00 per Watt in 2016 [2].

This exponential decrease makes solar energy attractive for a large variety of applications, such as building design. Especially for newly designed buildings it is relevant to look at Building Integrated Photovoltaics (BIPV) rather than Building Attached Photovoltaics (BAPV). Where the latter mainly focusses on attaching PV panels to existing building elements, such as rooftops, the former seeks to implement photovoltaic (PV) technology into the building at its construction. Thereby, it can be done in a more efficient manner as it can be taken into account in the designing phase which gives multiple functionality to PV panels, using them for energy production, as structural elements, and with the proper design even the heat produced by the solar cells could be utilised.

1.1. Temperature dependence of photovoltaics

Even though PV panels can absorb approximately 80% of the incident solar radiation, the most commonly used commercial PV panels only have a nominal efficiency of around $10-20\%$. Most of the energy absorbed is thermalised by the solar cells, meaning that most of the absorbed solar radiation is translated into heat rather than electricity. This large fraction of heat dissipated in the solar cells can cause the panel temperature to rise far above the ambient temperature. On a sunny day the module temperature can rise about $20-30°C$ above ambient [16].

A rise in temperature causes a decrease in power output and thereby efficiency of $0.40-0.65\%/°C$ above $25°C$, at which the nominal efficiency of a crystalline silicon (c-Si) solar cell is uasually given [25],[16]. For a $30°C$ rise, this means a decrease in efficiency of 19.5% compared to the efficiency at $25°C$, therefore significant improvements in efficiency can be made with proper thermal management. A module's capacity degrades 0.5% for each year in operation, lab testing has shown that the degradation rates almost double for every $10°C$ increase in operating temperature [14], [10]. This means a module operating at a higher temperature has a significantly shorter life time.

Thermal management of PV modules can have significant benefits in both the improvement of the electrical efficiency and the prolonging of the operational life time. Additionally, the excess heat taken away by thermal management techniques can be useful when considered in a BIPV system, for example in heating, ventilation, and airconditioning (HVAC) applications.

1.2. Thermal management methods

To cool the PV panels down there are different thermal management techniques available, namely: natural convection, forced convection, water cooling, heat pipes, and phase change materials (PCMs). Different aspects of these techniques are show cased in table 1.1: cost, maintenance, energy consumption, thermal performance, heat storage, weather dependence [6], [7], [8]. In the following subsections these methods are shortly explained and the pros and cons are highlighted.

Table 1.1: Advantages and disadvantages of different thermal management techniques, adaptation from [6], [7], [8].

Method	Natural convection	Forced convection	Water cooling	Heat pipes	PCM
Cost	Low	Moderate	High	Low	Moderate
Maintenance	Low	Moderate	Moderate	Low	Low
Electricity consumption	No	Yes	Yes	No	No
Thermal performance	Low	High	High	Moderate	High
Weather dependence	High	Low	Low	Moderate	Moderate
Heat storage	No	No	Yes	Yes	Yes

1.2.1. Natural convection

Natural convection cooling means to let the air flow pass the module naturally. Sometimes heat fins are used to improve the rate of heat extraction. For BIPV, air inlets and outlets are required to make sure air can flow on both sides of the module. This is a cheap and simple method as little to no extra construction is required. However, this method is also limited in its thermal performance since air has a low density, low heat capacity, and low thermal conductivity. Another large disadvantage is that natural convection is largely dependent on wind speed and direction.

1.2.2. Forced convection

By regulating the air flow along the PV modules, it can be more effectively cooled than with natural convection. However there are still limitations due to the thermal properties of air and only minimal heat storage is possible. For this reason water and other cooling fluids with better thermal properties are used, however this comes at a higher cost. Disadvantages of forced convection cooling are the initial investment and maintenance costs, and as this is an active method of cooling, the electricity consumption of the cooling system will reduce the overall efficiency.

1.2.3. Water cooling

The temperature can be more precisely regulated by the use of water cooling by flowing water in channels along the back of the panel. The heat transfer rate of this method is higher compared to that of natural or forced convection, as water or other fluids have more beneficial thermal properties, as well as a higher density. The initial costs are high due to the pumps and pipes required for such a system, also the electricity consumption is higher than that of forced air. This method has the added benefit of producing warm water, which can be used for other purposes.

1.2.4. Heat pipes

Heat pipes can be used as a passive way of cooling when combined with natural convection, it can reach a better thermal performance than natural convection alone. However, it suffers from the same drawbacks such as low heat transfer of air and the high dependence on wind speed and direction.

1.2.5. Phase change materials

Phase change materials (PCM) use the latent heat of their phase change from solid to liquid to store heat from the PV panel while keeping the temperature around their melting point. This method has a higher heat storage when compared to air or water circulation methods due to latent heat absorption. However, if all the PCM is molten it will just act as a heat sink and is no longer effective at cooling. It has a relatively high cost compared to other passive convection methods. Furthermore, some PCMs can be toxic or corrosive which may cause disposal problems at the end of their life time and containment problems. However, among the passive solutions, PCM is the most promising when it comes to thermal management, and multi functionality as the heat can be used.

1.3. Previous Work

This research is a follow up on the work done by Chris Nierop y Sanchez, who has made a Comsol Multiphysics thermal model to predict the module temperature of a PV-PCM system [29]. In his work, he estimated that for an optimised PCM the peak operation temperature could be reduced by $4.5°C$ on an average summer day in Rotterdam, The Netherlands. Additionally, an experimental setup was also made and tested under a Large Area Steady State (LASS) solar simulator, here the PCMs were able to reduce the average module temperature by $30-36°C$ compared to a a similar model without PCM as shown in figure 1.1 [29]. However, this research was only done on a labscale for short time periods of up to 30 minutes and this large difference was due to the excessive heat production by the LASS solar simulator.

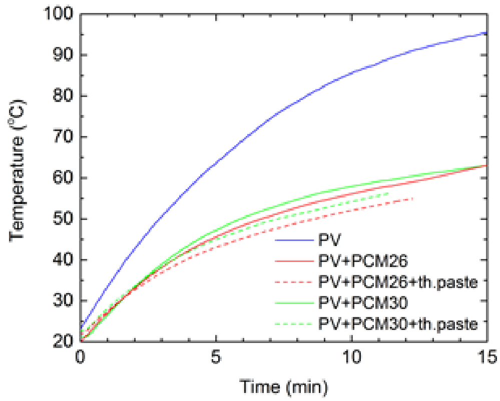

Figure 1.1: Temperature difference between modules with and without PCM under a LASS taken from [29].

Furthermore, an average peak time temperature drop of $10.5°C$ resulting in an 5.9% increase in yearly power output, was reported by A.Hasan et al. in the hot climate of the United Arab Emirates [7]. With simulations in the milder climate of Slovenia, R. Stropnik et al. have reported increases of 7.3% in annual energy production [28]. PCM cooling shows a lot of promise as it is a passive and relatively inexpensive method, with the added benefit that the stored heat can be used at a later time, for example at night when heating is required or for heating water.

1.4. Focus of this thesis

In this thesis the focus will be put on thermal management of PV modules by means of a phase change material. Currently PCM is already used in building insulation and thermal management to provide a heat buffer, to keep the temperature in a building stable [1]. The drawbacks of the research done in [29], are that the plane of array irradiance has not been taken into account, the time span of the experiments was short, and no real weather conditions were tested. Moreover, no long therm validation was done on the thermal model, and the module had large temperature fluctations due to the position of the junction box. Therefore, the goal of this research is to design a small PV-PCM module, placing the junction box so a large part of the solar cells can be covered by PCM slabs on the back. This module will then be used for long-term measurements during the summer of 2019 in mild climate of Delft, The Netherlands. Additionally, a thermal model will be made in Comsol Multiphysics whose parameters are as close to the experimental module as possible. By using both a Comsol Multiphysics thermal model and the outdoor experimental setup the model can be validated with the measurement results. Thereafter, it can be used to make predictions for the module temperature and optimisation of the PCM properties.

1.5. Outline of this thesis

This thesis consists of six chapters. In the first chapter, thermal management such as the temperature dependency of photovoltaics, different thermal management methods, the previous work, and focus and goals of this research were presented. In the second chapter, the necessary underlying theory is explained. The temperature dependence is explained, by looking at the effect temperature has on the following parameters: series resistance, short circuit current, and open circuit voltage. In this chapter an overview of the different heat transfer mechanisms is given, as well as the mechanism behind phase change materials how they are used in cooling, and how they can be modelled.

In chapter 3, the build up of the Comsol Multiphysics thermal model is discussed. This includes the geometry, material properties, heat transfer physics, and input data. Also the necessary assumptions made are highlighted. Furthermore, the effect of PCM parameters on the module temperature during a daily cycle are explored. Parameters included are latent heat, thermal conductivity, PCM thickness, and melting temperature.

Chapter 4 describes the construction of the modules and their characterisation under the LASS. The panels are checked for defects that may have occured during the construction using electroluminescence. Finally the thermocouples and their placement are described in this chapter.

The experimental results are presented in chapter 5, they are then compared to the results simulated with the Comsol thermal model and validated. Finally, this chapter looks into optimising the PCM parameters, thickness and melting temperature, to make predictions about the potential of PCM cooling on module temperature.

Finally, in chapter 6 the conclusions are drawn from the results and the important findings are explained. As well as, recommendations for future work are given.

2

Theory

In this chapter the underlying theory of the semiconductor and heat transfer physics used is going to be elaborated. Firstly the effect of temperature change on different parameters of photovoltaic cells will be discussed, followed by the relevant heat transfer mechanisms in a PV module. Finally, the working principles of phase change materials will be explained.

2.1. Effects of temperature on a photovoltaic cell

As a PV panel can reach up to $40°C$ above the ambient temperature [28], it is of great importance to know the effect temperature has on the different parameters of the cell. In this section the following three parameters are considered; series resistance, short circuit current, and the open circuit voltage.

2.1.1. Series resistance

The series resistance in a solar cell has three different causes; the movement of current through the emitter and base of the cell, the contact resistance between the metal contact and the silicon, and the resistance of the top and rear metal contacts [19]. The main effect of the series resistance is reduction of the fill factor as shown in figure 2.1.

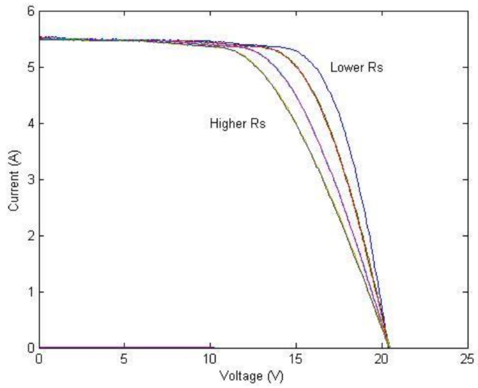

Figure 2.1: The effect of an increased series resistance on the IV-curve [12].

An increase in temperature induces an increase in lattice vibrations (phonons), which will affect the series resistance. These phonons can scatter the charge carriers and thereby decreasing their mobility [24], thus lowering the current. This influences the conductivity of charge carriers as shown in equation 2.1, where a lower mobility, μ, results in a lower conductivity. Since the resistance is given by $\rho = 1/\sigma$, a decrease in conductivity means an increase in resistance.

$$\sigma = e(n\mu_n + p\mu_p) \tag{2.1}$$

Between 300 and 350 K the r_s only increases a little, with the mobility being dependent of the temperature according to the relation shown in equation 2.2 [25].

$$\mu \propto T^{-\frac{3}{2}} \tag{2.2}$$

2.1.2. Short circuit current

The short circuit current, I_{sc}, is the current when there is no potential across the cell, if the cell is short circuited. The short circuit current depends on the flux of incident light. The short circuit current density, J_{sc}, is often used to remove the dependence on the cell area. It can be assumed to be equal to the photo generated current density as long as the photogenerated current is orders of magnitude larger than the recombination current due to thermal emission [9]. Therefore, the short circuit current can be approximated by equation 2.6[25]

$$J_{sc} \simeq J_{ph} = -q \int_0^{\lambda_G} \Phi_{ph,\lambda} d\lambda \tag{2.3}$$

The wavelength λ_G is the wavelength limit of photons that the cell can absorb to generate charge carriers, given by equation 2.4. It can be seen that the wavelength, λ_G, is inversely proportional to the bandgap E_G.

$$\lambda_G = \frac{h}{E_G} \tag{2.4}$$

The bandgap of a semiconductor tends to decrease with increasing temperature according to equation 2.5, where α and β are fitting parameters and E_{G0} is the bandgap energy at a reference temperature [30].

$$E_G(T) = E_{G0} - \frac{\alpha T^2}{T+\beta} \tag{2.5}$$

Therefore, the bandgap energy decreases due to an increase in temperature and as a result the maximum wavelength increases, which allows for additional photons to be absorbed. These photons will generate additional charge carriers and thereby increase the photo current, and thus the short circuit current.

2.1.3. Open circuit voltage

The open circuit voltage is the voltage at which no current flows through the external circuit, if the circuit is open. The open circuit voltage corresponds to the bias voltages where the dark current density, J_0, compensates the photocurrent density as shown in equation 2.6 [9].

$$J_{ph} = J_0 \left[exp\left(\frac{eV_{bi}}{kT} - 1 \right) \right] \tag{2.6}$$

$$V_{oc} = V_{bi} = \frac{kT}{e} ln\left(\frac{J_{ph}}{J_0} + 1 \right) \approx \frac{kT}{e} ln\left(\frac{J_{ph}}{J_0} \right) \tag{2.7}$$

The lowered bandgap caused by a rise in temperature as mentioned previously, lowers the barrier valence electrons needed to overcome by thermal activation. As a consequence, more of the valence electrons can cross the band gap to the conduction band, leaving behind an extra hole in the valence band. This increases the number of intrinsic charge carriers, both the holes in the valence band and electrons in the conduction band. These additionally generated charge carriers produce an increase in the dark current as shown by equation 2.8, where n_i is the intrinsic carrier concentration and the other variables are fundamental semiconductor properties namely, diffusion distance, diffusion coefficient and donor concentration [20]. The dark current is approximately equal to equation 2.9, where all the properties and constants are grouped under the single constant B' and γ is used to incorporate any temperature dependency of those properties.

$$J_0 = en_i^2 \frac{D_p}{L_p N_D} \tag{2.8}$$

$$J_0 \approx B' T^{\gamma} exp\left(-\frac{E_{G0}}{kT} \right) \tag{2.9}$$

Combining equations 2.7 and 2.9 gives an expression for the change of voltage due to the change in temperature as shown in equation 2.10.

$$V_{oc} = \frac{kT}{e} \left(lnI_{ph} - lnB' - \gamma lnT + \frac{eE_{G0}}{kT} \right) \implies \frac{dV_{oc}}{dT} = \frac{eV_{oc} - E_{G0}}{T} - \gamma k \tag{2.10}$$

Which means that the open circuit voltage will drop for an increasing temperature, in figure 2.2 the effect of a temperature increase on the IV-curve is shown. Here it can be observed that indeed the I_{sc} increases only slightly, whereas the V_{oc} decreases significantly causing a decrease in efficiency.

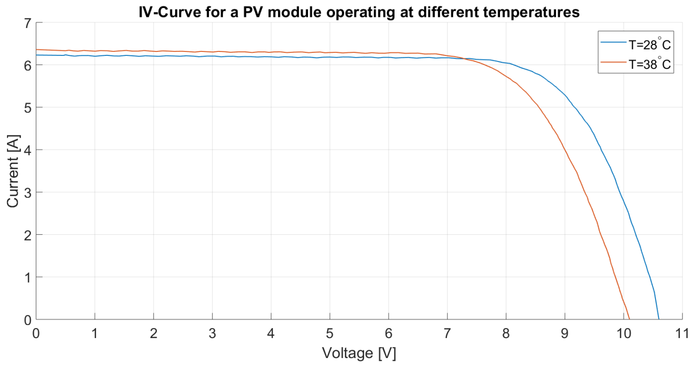

Figure 2.2: Effect of an increased temperature on the IV-curve of a solar cell.

2.2. Heat transfer

Heat transfer is an important part of this study, so to get a better understanding into how the different heat transfer methods work to obtain a PV module temperature, they will be shortly discussed in this section. The mechanisms are: conduction, convection, and radiation, they are graphically shown in figure 2.3. Lastly, the mechanism of phase change and how it can store heat will be discussed.

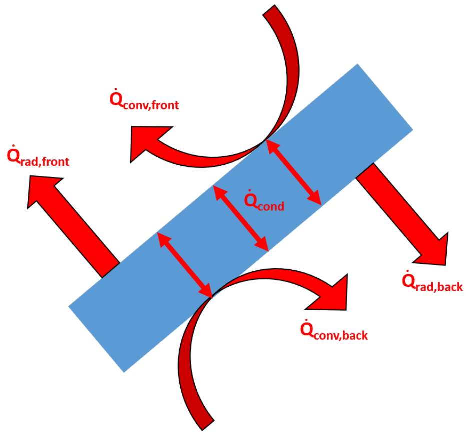

Figure 2.3: Schematic figure of all heat transfer mechanisms within a PV panel.

2.2.1. Conduction

Thermal conduction is the transfer of heat within a substance. This happens on a microscopic level by collisions between particles and movement of atoms. It is however not relevant in this research to look into the microscopic phenomena, but rather at the macroscopic effects that result because of it. The local heat flux through a homogeneous material is proportional to the negative of the local temperature gradient [23]. In a steady state this heat flux in one dimension is given by Fourier's law of heat conduction, equation 2.11, where $k[W/mK]$ is the thermal conductivity of the substance.

$$\dot{q}_{cond} = -k\frac{dT}{dx} \tag{2.11}$$

2.2.2. Convection

Convective heat transfer is the transfer of heat caused by the movement of fluid. It is used to describe the heat transfer from a surface to moving fluid. This flow can be forced, by pumps, fans, or wind this is referred to as forced convection, or a flow can be driven by buoyancy forces due to differences in density that arise from temperature difference, this is called natural or free convection. In an external forced flow the rate of heat transfer is proportional to the difference in temperature between the surface (T_s) and the fluid (T_e). It can be approximated by Newton's law of cooling, equation 2.12, where q is the heat flux from the surface into the fluid, and $h_c[W/m^2K]$ is the heat transfer coefficient.

$$\dot{q_{conv}} = h_c(T_e - T_s) \tag{2.12}$$

A lot of factors influence the heat transfer coefficient, therefore it is generally a complicated function of module geometry, tilt angle, location, and also atmospheric conditions such as humidity, ambient temperature, wind direction, wind speed, and pressure play a role [23]. Therefore an approximation has to be made, this is further discussed in chapter 3 where different convection models are elaborated.

2.2.3. Radiation

Heat transfer by radiation is caused by the electromagnetic waves (or photons) absorbed by or leaving a surface. The flux of energy incident on a surface is called irradiance, $G[W/m^2]$, the flux of energy leaving a surface due to emission and reflection is called radiosity, $J[W/m^2]$. A black surface or black body is by definition a surface that absorbs all incident radiation, thus it has no reflection [23]. Therefore, all the radiation leaving the black surface is emitted by the surface, this is described by the Stefan-Boltzmann law, equation 2.13, where $\sigma \approx 5.67 \cdot 10^{-8}[W/m^2K^4]$ is the Stefan-Boltzmann constant.

$$J = \sigma T^4 \tag{2.13}$$

Real surfaces do not absorb all incident radiation and thus emit less radiation than black surfaces, the surface is then called grey. The fraction of black body radiation that does get emitted is called the emittance, ϵ, the radiosity of a grey surface is then given by $J = \epsilon\sigma T^4$. The heat flux from one grey surface to another and its denoted by equation 2.14, where $\mathscr{F}_{12}$ is the transfer factor, which is dependent on the geometry and the emittances.

$$\dot{Q_{12}} = A_1 \mathscr{F}_{12} \sigma (T_1^4 - T_2^4) \tag{2.14}$$

On the other hand when the radiative heat transfer is not towards a specific surface but towards the sky, equation 2.15 is used to describe the heat transfer, where T_s is the surface temperature and T_{sky} is the effective sky temperature. Here the sky temperature can be modelled as a function of the ambient temperature, which is further discussed in chapter 3.

$$\dot{Q_{rad}} = A\epsilon\sigma \left(T_s^4 - T_{sky}^4\right) \tag{2.15}$$

2.2.4. Phase change

A phase change material (PCM) is a material that will change its phase by absorbing or releasing heat, in this case between solid and liquid, around the operating temperature of the system. If a material changes phase, from solid to liquid, the heat energy added to the solid will instead of creating a rise in temperature contribute to melting the material. Heat can thus be removed by a PCM in two ways; as sensible or latent heat. Here sensible heat raises the temperature of the PCM normally according to equation 2.16 (note: this also happens for non-PCMs), where $m[kg]$ is the mass of the material, $C_p[J/kgK]$ is the heat capacity, and the heat is a function of the temperature difference. Latent heat on the other hand is described by equation 2.17, where the specific latent heat $L_h[J/kg]$ is a material property.

$$Q_{sen} = mC_p(T_e - T_{PCM}) \tag{2.16}$$

$$Q_{lat} = mL_H \tag{2.17}$$

In theory this phase change happens at a constant temperature (T_{trans}). However, in practice the PCM is not isothermal so the phase change will happen over an interval (ΔT). Moreover, the temperature at which it happens depends on the direction of the phase change, from solid to liquid will happen at a higher temperature than from liquid back to solid. This is effect is called hysteresis [18]. In figures 2.4a the ideal case is shown and in figure 2.4b the effect of hysteresis is shown. The width of this interval depends on material properties, composition, and purity, for a material with more components it is generally larger than for a pure material.

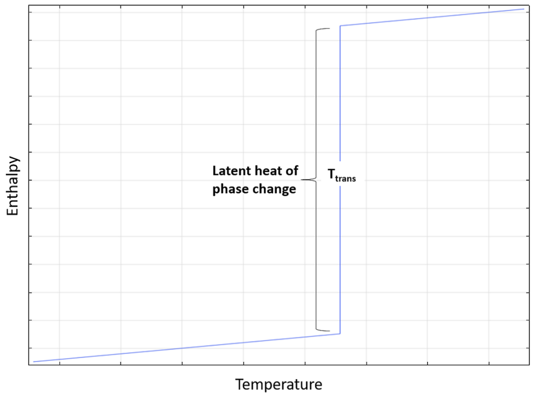

(a) Ideal isothermal phase change.

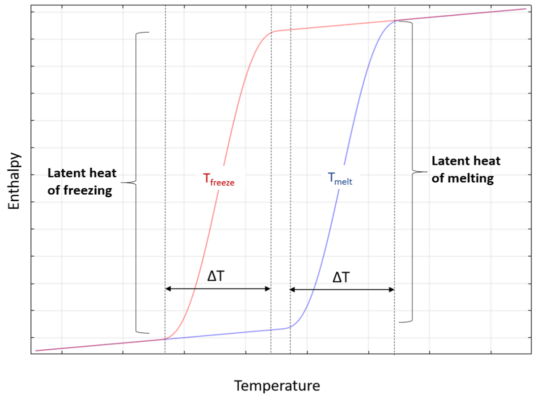

(b) Non-isothermal phase change with hysteresis.

Figure 2.4: Enthalpy of a phase change with and without hysteresis.

3
Thermal Model and PCM parameters

The simulations for this thesis are done in *Comsol Multiphysics 5.4*, where a one dimensional model of the cross-section of a PV module is build and simulated. In this chapter a short description of the numerical method Comsol uses for its calculations is described, then the steps and assumptions made in the model will be described. The model is build up in the following steps: geometry, materials, heat transfer physics, input data. Thereafter, the thermal model is used to study the effects of changing different PCM parameters on the module temperature. The following parameters are tested: latent heat, thermal conductivity, PCM thickness, and melting temperature.

3.1. Numerical method

Comsol Multihphysics uses a finite element method (FEM), to solve the heat transfer equations mentioned in chapter 2. Where a mesh is created of a continuous domain, and divides it into discrete subdomains called elements. For every element the equations and boundary conditions are then solved to come to an approximate solution. For more detailed information on how the Comsol Multiphysics numerical method works refer to [4].

3.2. Geometry definition

Firstly Comsol requires a geometric description of the module. To keep down computation times the module is modelled as a one dimensional cross-section, where every layer in the module is an interval of a certain length. The cross-section is based on the panels that will be designed for the measurements done in this research to keep the dimensions and materials used in simulation as close to what is actually used in the module. Three different models are build: one without a PCM, to be used as reference, which is build up with the following layers: Glass, EVA, Silicon, Copper, EVA, Tedlar. The second model is build similarly, however behind the tedlar layer, extra layers are added: polyethylene terephthalate plastic (PET), PCM, PET. The first model is described by the PV module part of figure 3.1 and the full module has the PCM slab attached behind it as shown in the full figure 3.1. Then the third is identical to the second model except that thermal paste is added between the tedlar and PET layer.

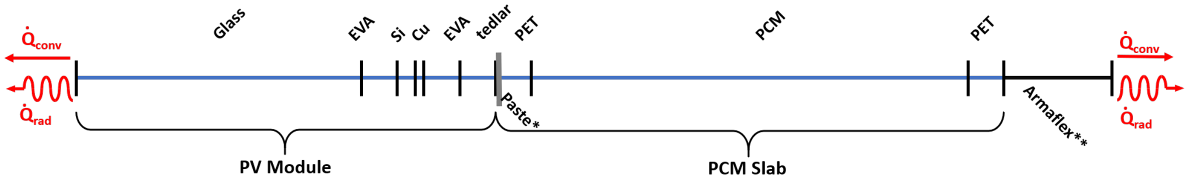

Figure 3.1: Cross-sectional model of a PV module with a PCM slab attached to the back, as it is used in the simulations (not to scale).*:Only added for PCM+T module. **:Added for the second set of simulations.

After the first measurements it was decided that BIPV conditions had to be emulated more accurately. This was done by attaching insulation material (*Armaflex*) to the back side of the modules, limiting the convective cooling. To accomplish this in the thermal model an extra layer of *Armaflex* insulation material is added behind the tedlar and PET layers for the PV and PV-PCM systems respectively. The thicknesses used in the simulations are shown in table 3.1, where the PCM thickness is variable and its importance will be discussed in later chapters.

3.3. Material properties

Once the geometry is build the relevant materials and their properties necessary to simulate heat transfer by conduction inside the module are added namely; density (ρ), heat capacity (C_p), thermal conductivity (k) and for the radiative cooling at either side of the module the emissivity (ϵ) is required for the front and back surfaces. The material properties are tabulated in table 3.1.

Table 3.1: Material properties of the PV module used for the Comsol model.

Material	ρ $[kg/m^3]$	C_p $[J/kg\cdot K]$	k $[W/m\cdot K]$	ϵ [-]	d $[mm]$
Glass	3000	500	1.8	0.93	40
EVA	935	480	0.34	-	0.45
Silicon	2329	700	131	-	0.180
Copper	8960	385	400	-	0.004
Tedlar	1200	1250	0.2	0.89	0.5
Thermal Paste	2600	1200	3	-	0.200
PET	1380	1000	0.15	0.90	0.4
Armaflex	96	1000	0.037	0.80	19

Then the PCM with hysteresis is defined, where the phase change is modelled as a smoothed step function over a temperature interval as described in [18] and shown previously in figure 2.4b. The interval, ΔT, depends on the PCM material used, this range is found to be around $4°C$ for the PCM used [29]. The PCM properties are shown in table 3.3.

3.4. Heat Transfer Physics

Once the materials and their properties are added, the physics module for heat transfer in solids is added to the module. This will automatically apply the heat transfer coefficients of the materials to their respective domains. On the front and back side boundary conditions are added; convection and radiation based on equations 2.12 and 2.15 respectively. Since the absorption of the glass and EVA, is mostly in short wavelengths ($< 400nm$) and the AM1.5G spectrum is low for those wavelengths, it is shown that most heat is generated in the silicium layer [29]. When an electrical efficiency of 20% is assumed this means that 80% of the incoming irradiance is turned into heat. Hereby we neglect the reflection and absorption of the of the glass and EVA layers. This is modelled by adding a heat source in the silicon layer which produces heat based on a fraction (0.8) of the input irradiance. This choice is made for model and computational simplicity.

3.4.1. Convection

As mentioned in chapter 2, the convection coefficient, h_{conv}, is often a complex function of geometry, wind speed and direction, module position and tilt. Therefore, several different models for the convection coefficient are proposed based on findings in literature. From this the best fit can be chosen for the validation of the simulation with the experimental results. Most models found in literature are determined empirically, often the heat transfer coefficient h is described by the linear (for $n = 1$) or exponential equation 3.1, where a, b, and n are the determined parameters and U is the wind speed [26][17].

$$h = a + bU^n \tag{3.1}$$

Other empirical models incorporate the dimension of the module in the form of equation:

$$h = a + bU^n L^{-m} \tag{3.2}$$

To see the effect of the different convection models simulations were done to illustrate the different effect each model has on the module temperature of both a PCM module and a reference module. The convection models are tabulated in table 3.2. In figure 3.2a and 3.2b the results of these simulations are plotted, it can be observed that different convection model can have quite a different effect on the module temperature. Therefore, it is important that attention is given to the convection in both the simulation models and in the experimental setup.

Table 3.2: Different empirical convection models.

Equation	Reference
$h_{arici} = 8.91 + 2U$	[13]
$h_{sartori} = 5.74U^{0.3}L^{-0.2}$	[26]
$h_{sharples} = 9.4U^{0.5}$	[15]
$h_{duffie} = 5.7 + 3.8U$	[11]

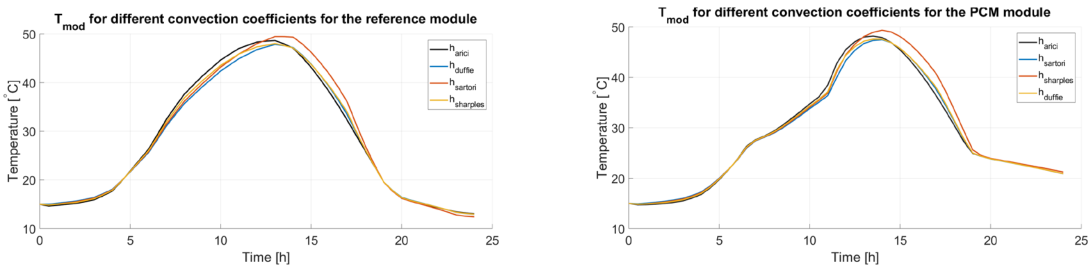

(a) Simulated module temperature for different convection models for a PV only module.

(b) Simulated module temperature for different convection models for a PV-PCM module.

3.4.2. Radiation

Next radiative cooling is added on the front according to equation 2.15, where T_{sky} is a model for the sky temperature as a function of ambient temperature given by equation 3.3. This equation is an estimate effective sky temperature for clear days based on [9]. Which means that it will underestimate the cooling during the night and overestimate the cooling during a cloudy day. During a cloudy day the effective sky temperature is approximately the ambient temperature $T_{sky} \approx T_{amb}$, because it is difficult to tell from data how cloudy it is and since clear days are when the most electricity is produced and thus also the most heat generated, this compromise is made.

$$T_{sky} = 0.0552 \cdot T_{amb}^{1.5} \tag{3.3}$$

On the back of the module it is assumed that the "T_{sky}", is equal to the ambient temperature. This compromise assumes that the surrounding background is equal to the ambient temperature, whereas in reality it depends highly on the albedo and temperature of the surroundings.

3.4.3. Weather data input

For the model to work accurately, weather data needs to be added. From this data the *Global Horizontal Irradiance (GHI)*, *Direct Normal Irradiance (DNI)*, *Diffuse Horizontal Irradiance (DHI)* are used to calculate the plane of array irradiance as described in appendix B, which together with the *Ambient Temperature* (T_{amb}), and *Windspeed (U)* are used as variable input for the model. The irradiance is used for the input of the heat source in the silicon layer as described previously. The wind speed is used to determine the convective heat transfer. The ambient temperature is used for the radiative as well as the convective heat transfer. For the outdoor measurements the same variables will be measured at the monitoring station, and will be used in validation and improvement of the model.

3.5. PCM properties

There are many types of materials that can be used for the purpose of cooling a photovoltaic module. In figure 3.3 it can be seen there is a wide range of different types of PCM and associated melting temperatures and melting enthalpy (latent heat).

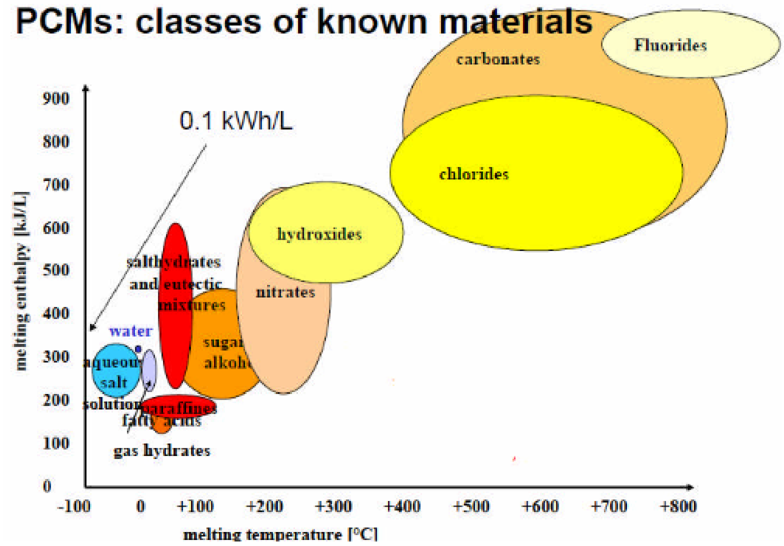

Figure 3.3: Melting temperature and melting enthalpy (latent heat) ranges of different types of PCM [22].

A PCM however will only be effective if its melting temperature is in the operating range of a PV module, choosing a melting temperature that is too low means it always remains in liquid phase and no latent heat can be stored. On the other hand having a melting temperature that is too high means it will never start melting and will always be solid. The typical PV module operation temperature is from around 10 to 60$°C$, depending highly on the location and season. The relevant melting temperature of the chosen PCM should be within this range, therefore the best suited material types are salt hydrates, paraffin wax, and fatty acids. Salt hydrates are inorganic ionic compound in which water molecules are enclosed within its crystal structure by ionic attraction. The have the general formula $M_xN_y.nH_2O$, where M is a metal ion and N is a non-metal ion. Most attractive properties are the high latent heat as shown in figure 3.3, relatively high thermal conductivity, and generally inexpensive. However, they can be corrosive to metals and during heating segregation between water and salt occurs [6]. Paraffin waxes are large carbohydrates with the general formula C_nH_{2n+2}, the advantages of which are non-toxic, no segregation, recyclable. However, they have a relatively low latent heat, low thermal conductivity, and are flammable [6]. Fatty acids are organic materials that can be derived from animal and vegetable fats, the main advantage is that they are sustainable materials which are non-toxic, non-corrosive, and are bio-degradable. However, their thermal conductivity and latent heat is generally lower than salt hydrates and paraffins as shown in figure 3.3. They all have their advantages and disadvantages, in this research salt hydrates were chosen as they have the highest latent heat and best thermal conductivity and showed the biggest temperature reduction according to [6]. The PCMs in this research were provided by the company *OC Autarkis* and their properties are listed in table 3.3 [1]. The parameters that will be optimised for are, the thickness and the melting temperature. Which are the properties that can be changed the easiest while having only a slight effect on the latent heat and thermal conductivity.

Table 3.3: Material properties of the PCM slabs used in both experimental and predictions.

PCM Components	$CaCl_2$, NH_4Cl, $SrCl_2$
Latent heat $[kJ/kg]$	178
T_{melt} $[°C]$	22-26
Density $[kg/m^3]$	1460
Thermal conductivity $[W/mK]$	0.57
Thickness $[cm]$	1.0

3.6. Effect of varying PCM parameters

This section will explore how changing different PCM parameters in the model will affect the module temperature during an arbitrary summer day in Delft. The ambient temperature and irradiance during this day are shown in figure 3.5. The parameters that will be looked at are; latent heat, thermal conductivity, PCM thickness, and transition temperature. Each time only one parameter is varied while the other parameters remain constant and the temperature is taken at two places, the back of the PV and the back of the PCM as shown in figure 3.4.

Figure 3.4: Two temperatures are taken: 1, the module temperature between the PV and PCM. 2, the back temperature behind the PCM.

A module without PCM is used as a reference and the initial temperature of the whole module is taken at 15 degrees Celsius. Furthermore, those parameters will be investigated to gain insight in the possibilities for optimisation and their limitations.

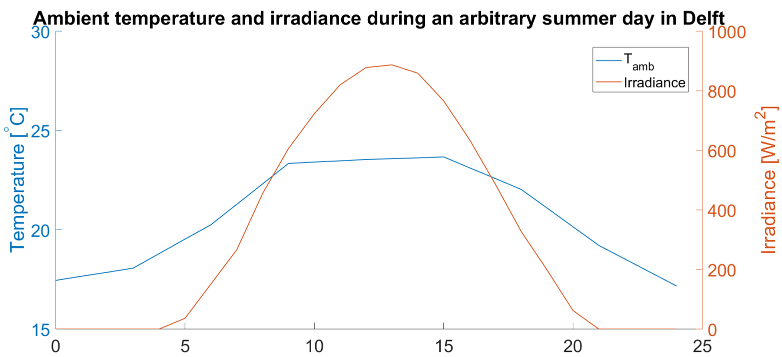

Figure 3.5: The ambient temperature and irradiance during the summer day used for the simulations.

3.6.1. Latent Heat

The latent heat, $L_H[kJ/kg]$, is the thermal energy which can be absorbed or released during a constant temperature phase transition process. It is a measure for how much energy it takes to change the phase of the PCM from solid to liquid. The module temperature, the temperature between the PV and PCM, is shown for different latent heat in figure 3.6a, similarly the temperature at the back of the PCM is shown in figure 3.6b. When looking at a simulation of a typical summer day for different latent heat. In figure 3.6a it can be seen that the temperature rises later on the day when it has a PCM attached. After approximately 10 hours the effect of different latent heat becomes more clear. For a higher latent heat the temperature stays lower for a longer time. However, during the cooling down stage it will stay at a higher temperature for a longer duration. If this cooldown period is too long it can negatively affect the next day, since the PCM is not fully reset to its initial state yet.

At the back of the PCM in figure 3.6b the temperature for higher latent heat will stay constant for a longer time, this indicates that it takes a longer time for the PCM with higher latent heat to melt completely. This confirms the expectation that more heat can be stored for higher values of latent heat. On the other hand, as also observed in figure 3.6a, for a higher latent heat the cool down period is longer, and therefore it might influence the following day, as the PCM is not completely solidified.

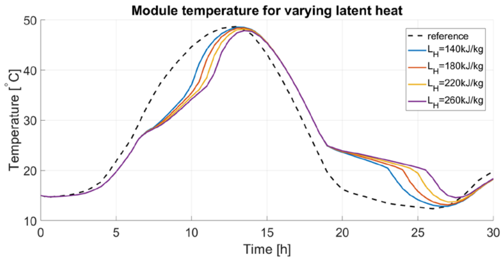

(a) Simulated module temperature between the PV and PCM for different latent heat.

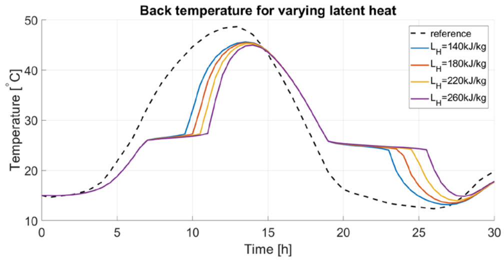

(b) Simulated temperature at the back of the PCM for different latent heat.

3.6.2. Thermal Conductivity

The thermal conductivity, $k[W/m/K]$, of the PCM is the rate at which heat can be transferred throughout the PCM. This will influence how quickly heat from the interface with the PV module can be transported away. Which is further stippulated in figure 3.7a, where for higher conduction the temperature starts rising later during the day.

At the back the opposite is therefore true as can be seen in figure 3.7b where the temperature rises earlier for higher conductivity than lower values. In practice however, it his hard to control the conductivity of the PCM, as this is a material property of the PCM. A way to make the PCM more conductive is by the use of highly conductive materials such as metals embedded in the PCM or the container, this is however beyond the scope of this research.

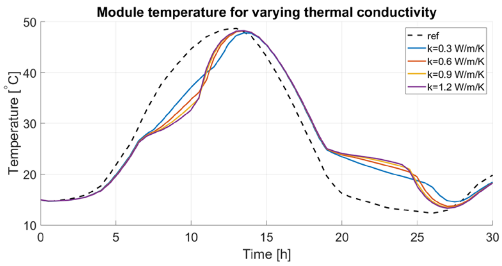

(a) Simulated module temperature between the PV and PCM for different thermal conductivity.

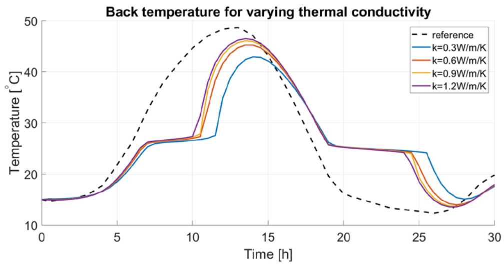

(b) Simulated temperature at the back of the PCM for different thermal conductivity.

3.6.3. PCM Thickness

The thickness of the PCM is a direct measure for the amount of energy that can be stored, as an increase in thickness will simply mean more PCM material. In figure 3.8a, it is observed that for thinner PCMs the temperature starts raising faster and earlier. However, for thick PCM layers there is hardly any difference after a certain thickness. The reason for this is shown in figure 3.8b, where the back of the PCM is not reached by the temperature change from the front. So further increasing the thickness will not improve the temperature as there is not enough heat to melt the

It is also witnessed that a thick PCM will have a larger impact on the following day as it takes longer to cool back down to the initial temperature. Therefore, it is important in optimisation that the PCM is able to solidify at the end of each day otherwise it will start acting as an insulator.

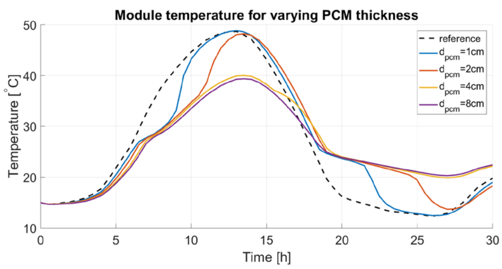

(a) Simulated module temperature between the PV and PCM for different PCM thickness.

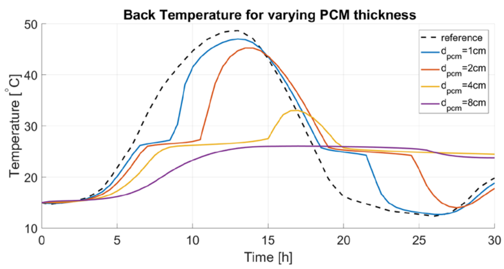

(b) Simulated temperature at the back of the module for different PCM thickness.

3.6.4. Melting Temperature

The melting temperature is the temperature around which the phase transition process of the PCM occurs. This happens over an interval rather than an exact temperature as explained previously in chapter 2. The melting temperature is defined as the middle of this temperature interval. The module temperature shown in figure 3.9a, shows that lower melting temperature means a larger temperature difference compared to the reference module early in the day. However it also means that the PCM is completely molten and the temperature will start rising earlier on the day. The temperature at the back of the PCM in figure 3.9b further shows this effect. Additionally, it is observed that for lower melting temperatures the PCM does not completely reset before the second day. A reason can be that the ambient temperature is higher than the melting temperature. This makes the melting temperature an important variable to optimise for every geographic location, season, and climate.

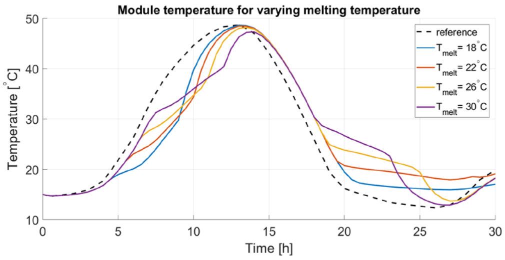

(a) Simulated module temperature between the PV and PCM for different melting temperature.

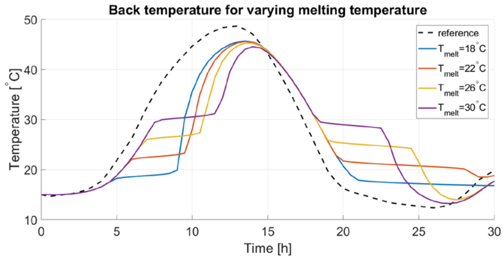

(b) Simulated temperature at the back of the module for different melting temperature.

4 Experimental Setup

In this chapter the design of the panel, including the reasons for redesigning will be explained. Furthermore, a description will be given of the construction of the panel. The characterisation of the modules is done and any defects are being looked at using electroluminescence. Finally, the thermocouple placement and their thermal deviations are described.

4.1. Module Design

The main reason a different module design is necessary from the standard commercially available panels is the position of the junction box. Since the junction box is generally located on the back of the module it can hinder the placement of PCM slabs and thereby the PCM coverage of the cells. This is displayed in figure 4.1, were the uncovered area is shown in red and the covered area in blue. During tests performed under a (LASS) by [29], in the red box temperatures of up to $30°C$ higher than in the covered blue areas were measured. Additionally, the PCM slabs could not be attached properly and space was left open between the back of the PV and the PCM hampering the thermal contact.

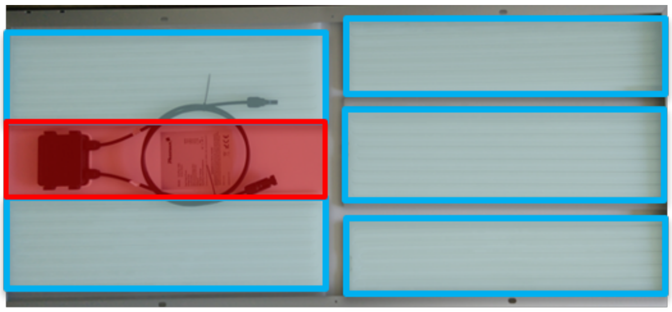

Figure 4.1: Hindrance of PCM placement due to the junction box, causing significant temperature differences within the panel [29].

The two challenges of the module design are: to get a sufficient coverage factor of the cells by better junction box positioning so that the junction box does not impede the PCM placement and additionally a better way of attaching the PCM slabs has to be constructed to increase thermal contact.

4.1.1. Coverage Factor

The goal is to maximise the fraction of the total panel area that is covered by solar cells. But more importantly, the PCM slabs have to cover as much of the effective area of the PV panel as possible. There are some restrictions as to what can be build with the facilities available, therefore the size of the panel is kept at $60x60cm$. The cells used are 5 inch Interdigitated back contact (IBC) cells, which have a special architecture with both contacts on the rear side of the device. This makes IBC cells easier to simulate thermally, as there is no metal fingers on the front and it can be simulated with two layers, a silicium and a copper layer (as described in chapter 3). The cells can be connected to each other from top to bottom as shown in figure 4.3, using a single connector. For the front glass pane a textured low iron solar glass is chosen, which has a higher transmittance than regular clear flat glass. As the connections are on the bottom of the cells, it is impossible to cut the cells to shape. Therefore, it was determined that a 4x4 cell layout is the maximum obtainable number of cells on a $60x60cm$ panel leaving room for connections and junction box. This layout is schematically shown in figure 4.2, where the junction box position is drawn, however the junction box is on the rear side of the panel.

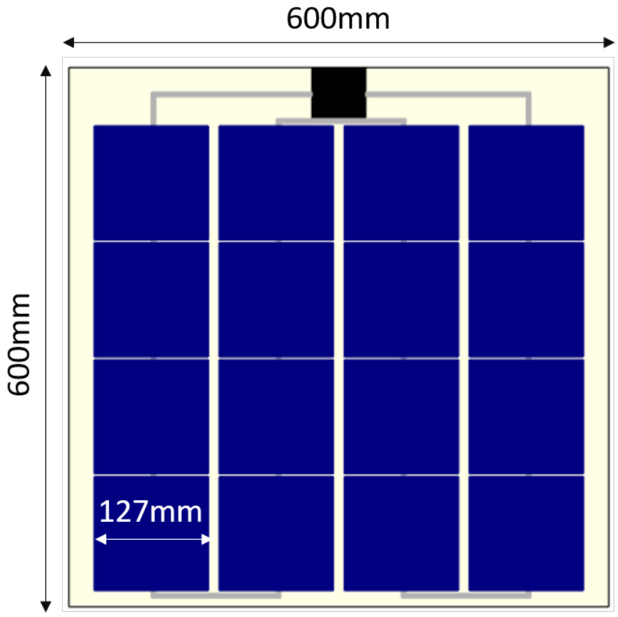

Figure 4.2: Schematic of the panel layout using 5-inch IBC cells in a 4x4 grid, with a small junction box.

4.1.2. Construction

The construction of the module is straight forward, firstly the IBC cells are soldered together in strings after which the strings are attached to eachother, the result can be seen in figure 4.3. After this the connections that will later go to the junction box are made.

Figure 4.3: IBC cells connected in a single series string.

Then the module layers are stacked upside down on top of the front glass pane in the following order: glass, EVA, cells and connection wires, EVA, and tedlar backsheet. Thereafter, the stacked layers are placed into the laminator, shown in figure 4.4a. Here heat and pressure is applied, the heat will melt the EVA and the pressure will then squeeze everything together keeping it in place and making it a single coherent piece. The resulting module is shown in figure 4.4b.

(a) Laminator capable of producing $60x60cm$ panels.

(b) Laminated panel without junction box.

Figure 4.4

From the junction box the bypass diodes are removed, since the panels are small and their cells are not connected parallel, the bypass diode has no function and will only cause current leakage. Moreover, the maximum voltage is significantly lower than that of a regular solar panel since the number of cells is only 16 per module rather than 60 or 72 for regular panels. The junction box is then installed at the rear of the panel so it can be connected safely. The junction box is glued on with super glue and sealed on both the inside and outside with silicone, to create a watertight seal as shown in figure 4.5. Three modules were constructed this way to be used as follows: one as reference, one with PCM at the back, and the third with a layer of thermal paste between module and PCM. These modules are then characterised as described in the following section.

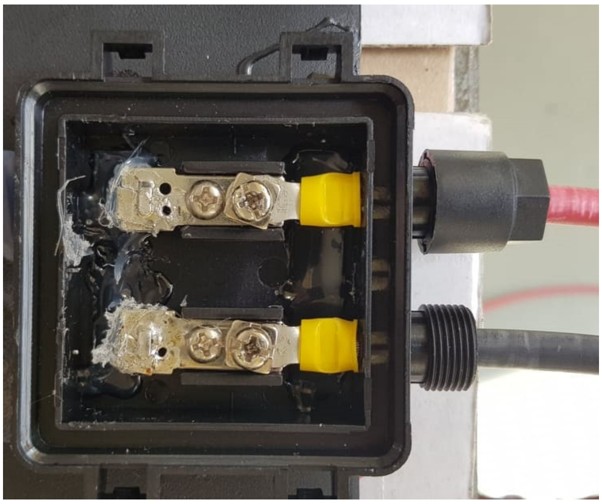

Figure 4.5: The junctionbox is super glued to the back of the panel, and sealed with silicone from both in and outside.

Finally, an aluminium frame was built so the modules can be attached to the rack on the rooftop monitoring station. The frame can be seen in figure 4.6, here the aluminium bars across the back of the modules push the PCM slabs onto the module and hold the modules in the correct vertical place in the frame. Thereby, creating a good thermal contact between PV and PCM additionally, this will hold the PCM slabs in place. The thermocouples are installed on the rear of the panels before the PCM slabs are attached.

4.2. Characterisation

In this section the modules are characterised to see how they perform under a LASS. Panel 1 will later on be used as reference module, panel 2 will be used with PV-PCM and panel 3 will be PV-PCM with a layer of

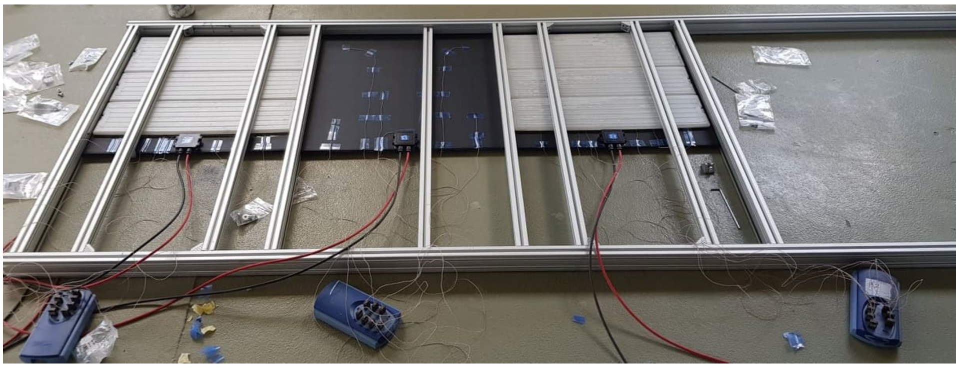

Figure 4.6: The modules are placed into an aluminium frame, which serves a dual purpose of allowing attachment to the rack and holding the PCM slabs in place.

Figure 4.7: Rooftop monitoring station rack with the three modules attached.

thermal paste in between. Their electroluminescence pictures are taken to see if any defects have occured during the construction.

4.2.1. Module parameters

As can be observed from the IV-curves of the three modules, shown in figure 4.8, there are slight differences between the panels. Their parameters are summarised in table 4.1. Here panel 1 has a slightly higher short circuit current and a lower open circuit voltage, compared to the other two panels. This difference can however be explained largely by the difference in module temperature during the measurement, since an increase in temperature causes a slight increase in current, but a significant decrease in voltage, as explained in chapter 2. Taking this into consideration the panels' parameters are close enough to make proper comparisons between them.

Table 4.1: Parameters for all three modules as measured under the LASS.

Parameter	**Panel 1 (ref)**	**Panel 2 (PCM)**	**Panel 3 (PCM+T)**
V_{oc} $[V]$	10.68	10.74	10.79
I_{sc} $[A]$	6.18	6.15	6.09
P_{mpp} $[W]$	48.35	48.7	48.6
FF	73.22	73.75	73.98
η [%]	19.75	19.91	19.84
Module Temperature	25.0	24.1	23.8
Irradiance $[W/m^2]$	970	974	978

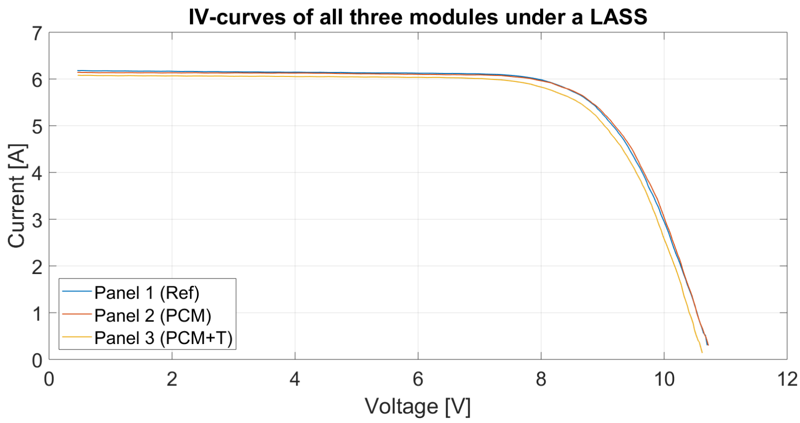

Figure 4.8: IV-curves for the different modules under the LASS.

4.2.2. Electroluminescence

By feeding current into a module the cells will start acting like a large area LED, by emitting light with an energy around the band gap of the semiconductor, this effect is called electroluminescence and a picture of this light can be made. Since the band gap of silicon is around 1100nm this is not visible light, but infrared (IR). An IR image can then be made, which provides information about the uniformity and defects in the cells. In figures 4.9a, 4.9b, 4.9c the electroluminescence pictures of panels 1,2, and 3 are shown, respectively. It can be seen that there are dark spots at the edges of each cell, caused by the soldering of the connectors on the back. The remaining parts of the cells, however are uniform which indicates that during the construction no significant defects were formed.

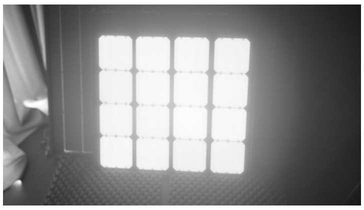

(a) Panel 1

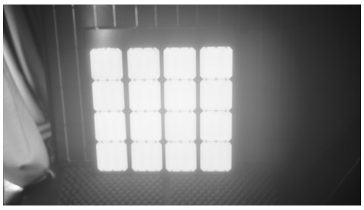

(b) Panel 2

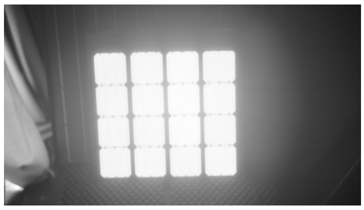

(c) Panel 3

Figure 4.9: Electroluminescence pictures of the three modules.

4.3. Measurement

The measurements are done in Delft at the PVMD Monitoring station, where weather and power output data is collected every 10 minutes. The equipment used at the monitoring station are fully described by M. Keijzer in [21]. The equipment used specifically for this project are thermocouples, the use of which will be described in the following section.

4.3.1. Thermocouples

To measure the module temperature, thermocouples are placed on the backside of the module. For the PV-PCM panels this means that they are in between the panel and the PCM slabs. The thermocouples that are used are T-type thermocouples.Tthe data is logged via *TC-08 Thermocouple Data Logger* via the encompanying *PicoLog 6.0* software. Every ten minutes a data point is made by taking the average over the past ten minutes, this data point is stored locally on a Raspberry Pi. The Data Logger has eight channels, out of which seven are used to collect data, these seven thermocouples are placed in the configuration as shown in figure 4.10 the red boxes represent the measured cells and the blue boxes represent the unmeasured cells. Six out of the seven thermocouples are placed directly behind the center of a cell, the average of the data from these is used in the analysis.

Furthermore, to gain insight in the temperature deviation on different locations on the panels, the deviation of each separate thermocouple from the average of all thermocouples is calculated over the period from

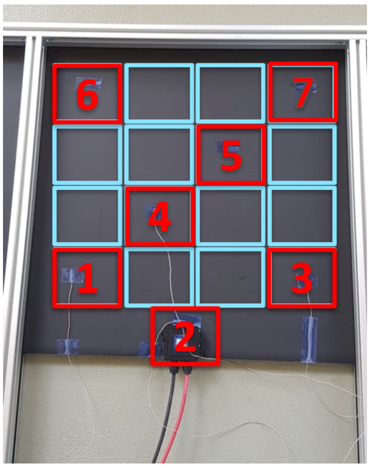

Figure 4.10: Illustration of the position of all the thermocouples at the back of the modules in red and the unmeasured cells in blue.

2-22 July. The results are shown in figure 4.11, it can be seen that the differences between each thermocouple are the largest for the reference panel. This is likely due to convection as the thermocouples are unprotected from the wind on the back side, in contrast to the PV-PCM modules where the PCM slabs shield the thermo couples from the wind since they are attached between PV and PCM. The standard deviations from the average are $1.68°C$, $0.77°C$, $0.92°C$ for the reference, PCM, and PCM+T modules, respectively. Therefore, temperature difference due to location on the panel is minimal. Furthermore, according to the manufacturer the error of the thermocouples is $\pm 0.5°C$.

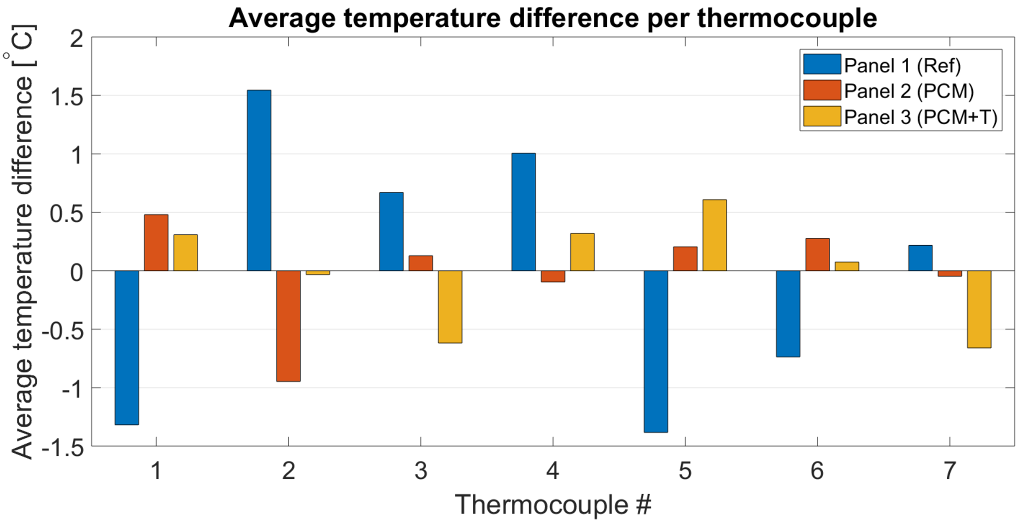

Figure 4.11: Temperature deviation of each thermocouple from the average temperature over all thermocouples.

5

Results, Validation & Predictions

In this chapter the measurement results will be shown and then will be compared to the simulation results to validate the thermal model. The thermal model is thereafter used to make predictions for longer periods based on different weather data sets. This is then used to obtain optimal parameter settings for the PCM thickness and melting temperature, to predict the temperature decrease and electrical yield gain that can be accomplished by using PCM thermal management. This is done for two different setups; firstly the free standing rack mounted pv panels, secondly insulating material is added on the back of the modules to emulate BIPV conditions.

5.1. Free standing rack

This section will discuss the rooftop measurement results for the three different panels, where they are mounted on a free standing rack with no insulation at the back side. Then, compare those results to the simulation results for different convection models to see which model has the lowest error and is thus the best fit. Finally, predictions are done for three different weather data sets, for the measured weather data that was done on the rooftop monitoring station in Delft during July 2019 from the 2^{nd} until 22^{nd}, for the month July of the typical meteorological year data of Delft from PVGIS [3], and for the month of July of the PVPortal climate data of the Rotterdam KNMI weather station (the closest weather station to Delft).

5.1.1. Results measurement

Calculating the effective temperature difference according to the method described in appendix A, gives an effective average temperature difference of $0.521°C$ and $2.50°C$ for the PCM and PCMT modules respectively over the whole period from 2^{nd} until 22^{nd} July. The peak temperature difference found between the reference and PCM module was $-9.66°C$ at 1:20pm. In figure 5.1 the results from 2-8 July are shown to gain insight in the main trends over five daily cycles. At the end of each day the temperature for the PCM and PCMT modules stays higher for some hours, this is caused by the solidification of the PCM slabs as predicted in chapter 3. Another trend that is observed, is that in general the PCM and PCMT temperature is greater than the reference temperature. However, at the start of the day a slight decrease in temperature is seen, a good example of this decrease is seen during the 4^{th} of July in figure 5.1, this decrease can be associated with the melting of the PCM. This suggests that the PCM is might be cooling the module, but the cooling effect is not as large as expected. furthermore, the thermal paste is not having the desired effect of improving the heat transfer towards the PCM, as the module with thermal paste has a higher module temperature during the day.

A reason for this behaviour can be that because the panels' back sides are exposed to the wind, the convective cooling on the reference module is larger than the cooling provided by the PCM. So in this case the PCM is mostly just acting as an insulator, and the thermal paste is increasing the insulation of the backside even moreso. Additionally, the heat storage capacity of the PCM slabs is too low to remove enough heat. However, the data can still be used to validate the thermal model and simulate different PCM parameters to see if a net cooling effect can be reached for these conditions.

Secondly, the energy produced by each module over the whole measurement period was calculated by intergrating the power produced over the time span. It was found that over this three week period the panels

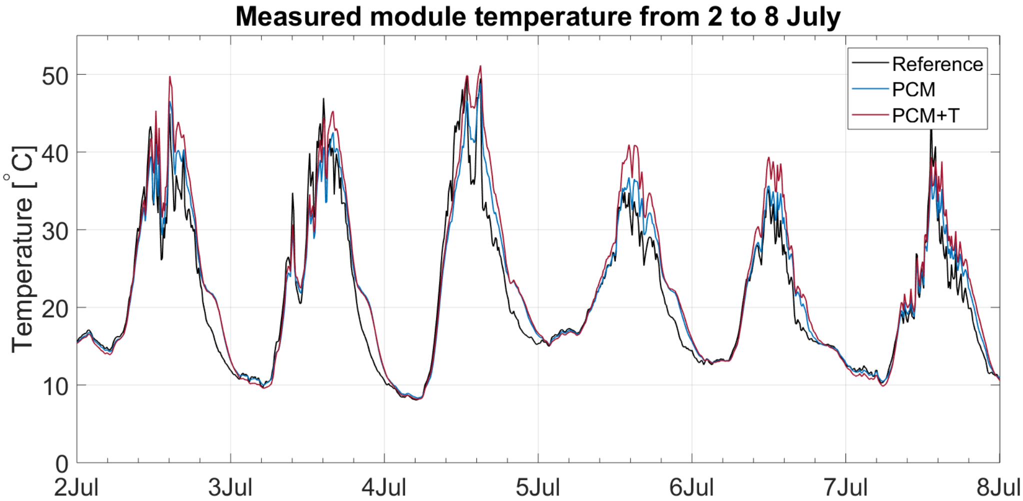

Figure 5.1: Measured module temperatures from 2 July until 8 July.

produced 5.037, 5.093, 5.040kWh for the reference, PCM, and PCMT modules respectively as tabulated in table 5.1. This implies that even though the module temperature of the PCM panel was slightly higher it still performed slightly better. The increased performance is only around 1% for the PCM panel so this can also be caused by other aspects (ie. the differences between the panels, and uncertainty in the measurement equipment) and is therefore inconclusive.

Table 5.1: Energy yield and percentage wise improvement over the measured period from 2-22 July without insulation.

Module	**Reference module**	**PCM module**	**PCM+T module**
Energy Yield [kWh]	5.037	5.093	5.040
Improvement	-	+1.1%	+0.06%

5.1.2. Validation

In order to predict the optimal PCM parameters, the thermal model needs to be validated. In chapter 3, four different convection models were proposed, see table 3.2, these models are all compared with the measured data. Figure 5.2 shows the module temperatures for the reference panel for both simulated and measured temperatures from the 4^{th} until the 8^{th} of July 2019. It can be seen that in general all models over estimate the temperature during the day slightly while underestimating the temperature at night. In general the models which have a larger wind speed component, Sharples and Sartori, make a larger overestimation and underestimation on the temperature than the other two models. Similar trends where found for the PCM and PCMT modules, the results of which can be found in Appendix D. Looking closely at the figure it seems that the Arici model is following the measured data the best, however to be certain the root mean squared error (RMSE) is taken between the simulated model and the measured data, the method of which is described in appendix C, this will provide insight in what model can make the most accurate predictions.

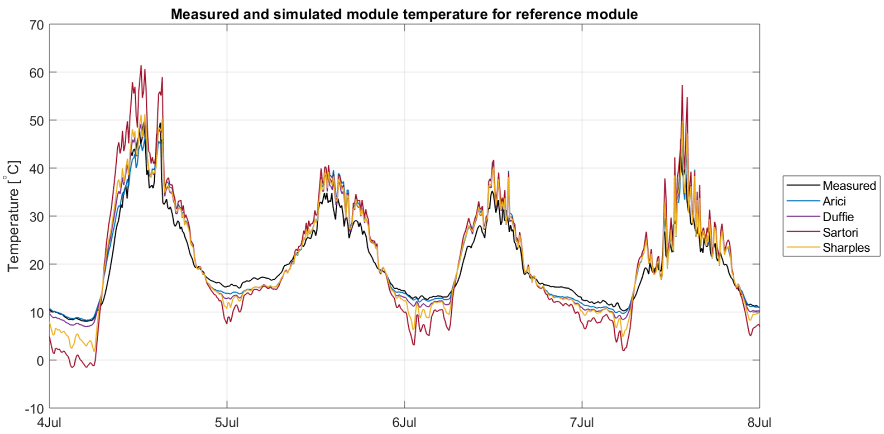

Figure 5.2: Comparison of the measured and simulated data from 4-8 July.

The RMSE values of all three modules of all convection models are tabulated in table 5.2. Which confirms that the Arici model is indeed the best fit, since it produces the lowest RMSE values. Therefore, it is the model chosen to make predictions using different weather data sets and PCM parameters to find to optimal parameter settings.

Table 5.2: Root mean square error values of different simulated models compared to measured values.

Convection Model	**Reference module** [$°C$]	**PCM module** [$°C$]	**PCM+T module** [$°C$]
Arici	2.46	2.28	2.55
Duffie	2.59	2.46	2.70
Sartori	5.26	4.19	3.91
Sharples	3.53	3.01	3.15

5.1.3. Predictions

Predictions are made for the PCM module only and with the Arici convection model. Three different sets of weather data: PVGIS, PVPortal, measured data. The PVGIS data uses a typical meteorological year in Delft for the period 2007-2016 [3]. The PVPortal uses the data from the closest KNMI weatherstation (Rotterdam) over the period 1991-2019 and averages it [27].

For each data set simulations were performed by varying the melting temperature from 20 to 25$°C$ with steps of 1$°C$ and varying the PCM thickness from 1 to 5cm using steps of 1cm. Then the temperature differences over the whole period were taken, and three best results for each dataset are listed in table5.3. All simulation models predict that some temperature decrease can be managed by PCM thermal management, however there is a difference between each dataset. A reason for this difference can be that the PVGIS and PVPortal data is taken hourly and the measured data is taken every 10 minutes. As a consequence the measured data has more fluctuations since the weather especially the wind and irradiance can fluctuate greatly, this can be seen from the graphs for three arbitrary days shown in figures 5.3, 5.4, and 5.5.

Table 5.3: Table with the top three PCM parameters for the PVGIS, PVPortal, and measured data.

	PVGIS	**PVPortal**	**Measured**
$d_{pcm}, T_{melt}, \Delta T$	$5cm, 23°C, -0.435°C$	$5cm, 21°C, -0.845°C$	$5cm, 23°C, -2.13°C$
$d_{pcm}, T_{melt}, \Delta T$	$4cm, 22°C, -0.410°C$	$4cm, 20°C, -0.735°C$	$4cm, 22°C, -2.09°C$
$d_{pcm}, T_{melt}, \Delta T$	$5cm, 22°C, -0.400°C$	$5cm, 20°C, -0.730°C$	$5cm, 22°C, -2.09°C$

Furthermore, all models predict that for a PCM thickness of $4-5cm$ the temperature decrease is the greatest as seen from table 5.3. However, the PVPortal data predicts an optimum for $20-21°C$ whereas the PVGIS and the measured data predict the best thermal performance at $22-23°C$. A reason for this difference can be because of the way the data set is created. As mentioned before, the PVGIS data is for a typical July in the period from 2007-2016, which therefore represents the weather actually measured during a month in this period. On the other hand, the PVPortal data uses all data from 1991-2019 and averages it. Meaning that the data no longer represents actual measured data but instead each data point is an average of 30 values, thereby creating an unrealistic temperature curve. This explains the smoother curves shown in figure 5.4 compared to figures 5.3 and 5.5, as indeed all the fluctuations are removed by averaging. Because the heat produced is a function of the incident irradiance in the thermal model, a lower amount of variation due to taking an average can cause a significant difference. Additionally, the PVPortal data is from Rotterdam rather than Delft. Therefore, the results from the PVGIS and measured data are more reliable and the optimal parameters for the thickness and melting temperature are expected to be close to $5cm$, $23°C$.

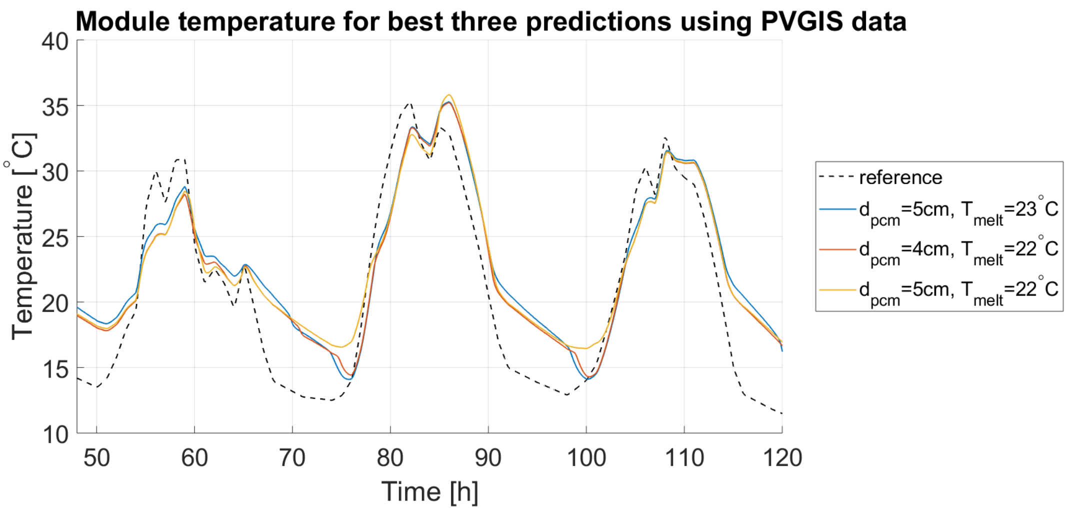

Figure 5.3: The predicted module temperature for the simulation results of the PVGIS data of three situations that produce the best thermal performance.

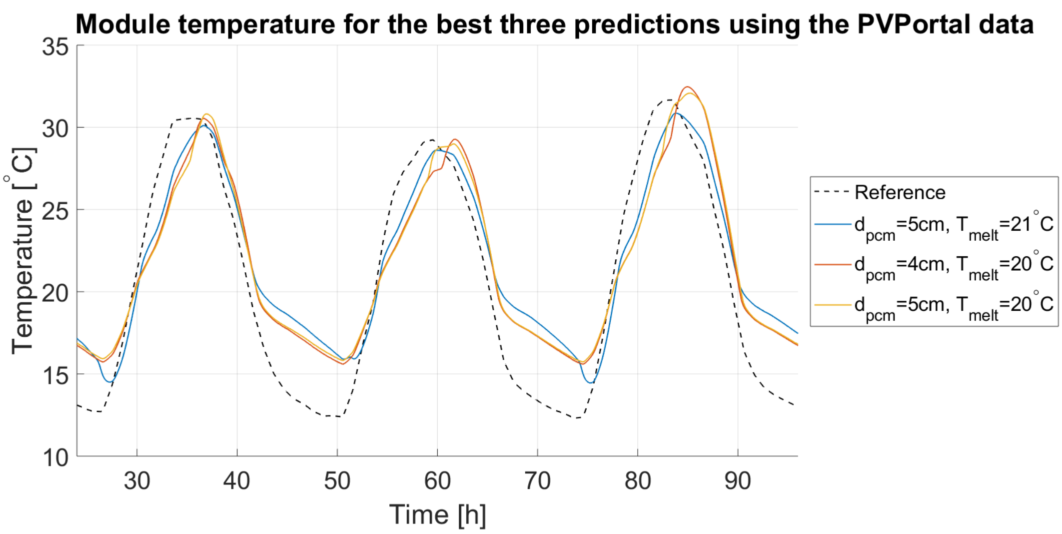

Figure 5.4: The predicted module temperature for the simulation results of the PVPortal data of three situations that produce the best thermal performance.

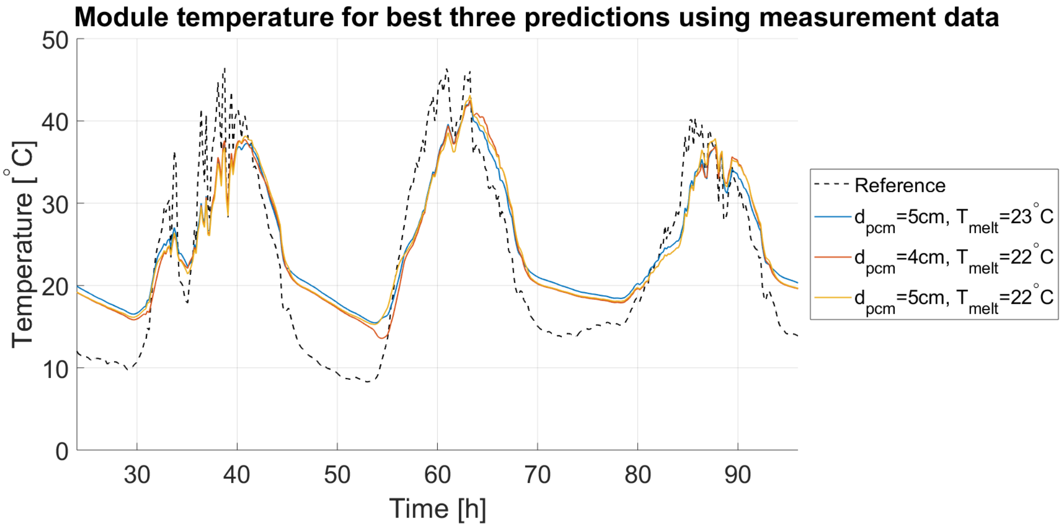

Figure 5.5: The predicted module temperature for the simulation results of the measured data of three situations that produce the best thermal performance.

5.1.4. Cold month

The best performing PCM parameters, a thickness of $5cm$ and a melting temperature of $23°C$, are thereafter simulated using the PVGIS data for a typical January, to see how the system performs in a cold month. In figure 5.6 the results of several days of the simulation are presented, it can be seen that the temperature differences are small the PV-PCM module's temperature curve seems to be lagging behind the reference module. This is likely caused by the PCM being slower to respond to temperature change as the PCM is not melting at these temperatures. Furthermore, during the night the temperature is even slightly lower than the reference module. All in all, the calculated temperature difference was found to be only $-0.5°C$ which means that attaching a PCM definitely does not have a negative effect during winter months.

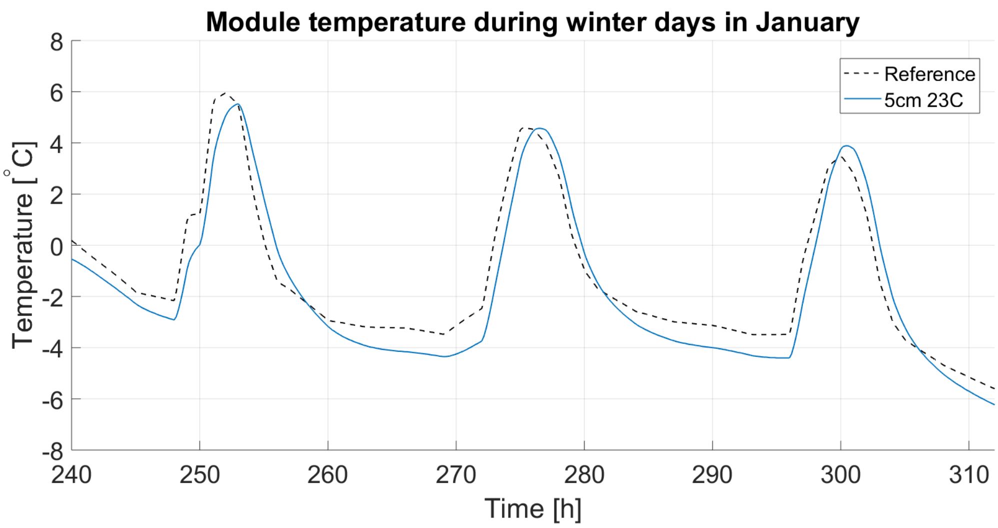

Figure 5.6: The predicted module temperature for several cold days in January using the predicted optimal parameters.

5.2. Insulated backside

Because in future research the Architecture department wishes to design a wall façade with an integrated PV-PCM system, the BIPV conditions need to be emulated more properly to make a meaningful comparison. Therefore, the back is insulated with *Armaflex* insulation material which will eliminate most of the convective and radiative cooling on the rear side. The measurements with an insulated backside were performed in the period, 26^{th} of July until 7^{th} of August.

5.2.1. Measurement results

Using the same method of calculating the difference in temperature as described in appendix A gives an average temperature difference, over the period from 26^{th} July until the 7^{th} August, of $-6.69°C$ for the PCM and $-5.09°C$ for the PCMT module. The peak temperature difference was found at 11:10am with a difference of $-21.7°C$. In figure 5.7 several days of the whole period are shown, it can be seen that during the day the temperature of the panels with PCM is lower than the reference panel. However, at night and in the evening the temperature of the PCM modules is higher due to the cooling of the PCM happening at a slower rate than without. In general the PCMT module is still performing worse than the PCM module, which implies that the thermal paste is not improving the heat transfer between PV and PCM, a reason can be that the layer of thermal paste is significantly thicker than advised the layer is around $200\mu m$ where the manufacturer advises using a layer of $20-40\mu m$ [5]. So instead of improving the thermal contact between PV and PCM it forms an additional thermal resistance.

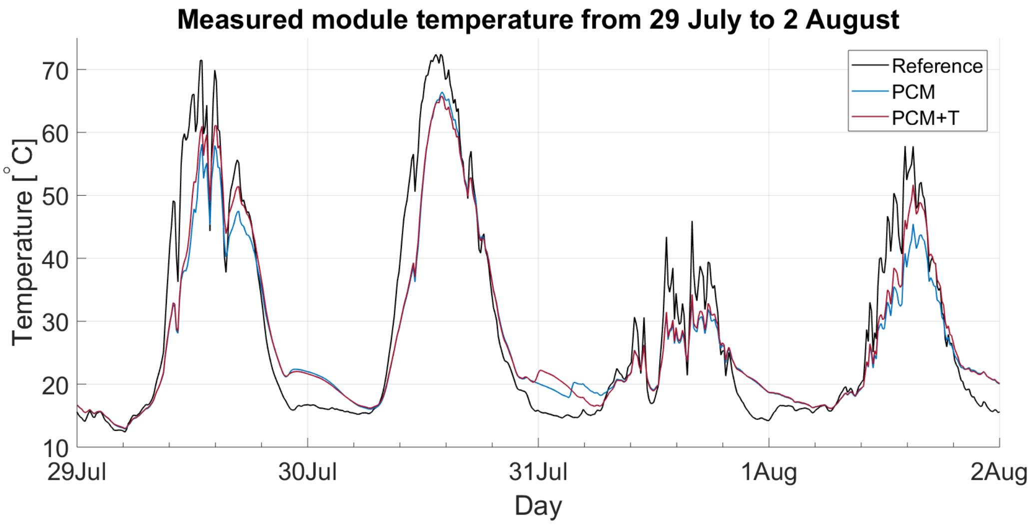

Figure 5.7: Measured module temperatures from 29 July until 2 August for all three modules.

Another observation that can be made is when comparing the results with and without insulation, it can be seen that the peak temperature of the reference module without insulation is around $50°C$ compared to peak temperatures of over $70°C$ with insulation. This gives an indication of the amount of cooling wind provided during the first experiment and also shows why especially in BIPV cooling is more necessary.

Looking at the energy yield over this measurement period it was found that the reference module produced 2.88 kWh, where the PCM and PCMT modules produced 2.96 and 2.92 kWh respectively, this is summarised in table 5.4. This means that the PCM panel has a 2.8% and the PCMT panel a 1.4% increase in performance with respect to the reference panel.

Table 5.4: Energy yield and percentage wise improvement over the measured period from 26 July - 7 Aug with insulation.

Module	**Reference module**	**PCM module**	**PCM+T module**
Energy Yield $[kWh]$	2.88	2.96	2.92
Improvement	-	+2.8%	+1.4%

5.2.2. Validation

For validation of the thermal model with insulated back, firstly the graphs are looked at to see how well the simulated data follows the measured data. In figure 5.8 a comparison between the measured and simulated module is shown for three days. Here, it can be seen that the simulation follows the measured curve reasonably well, however during warm days the thermal model underestimates the temperature around midday. Additionally, during the night there is again a slight underestimation as was seen previously.

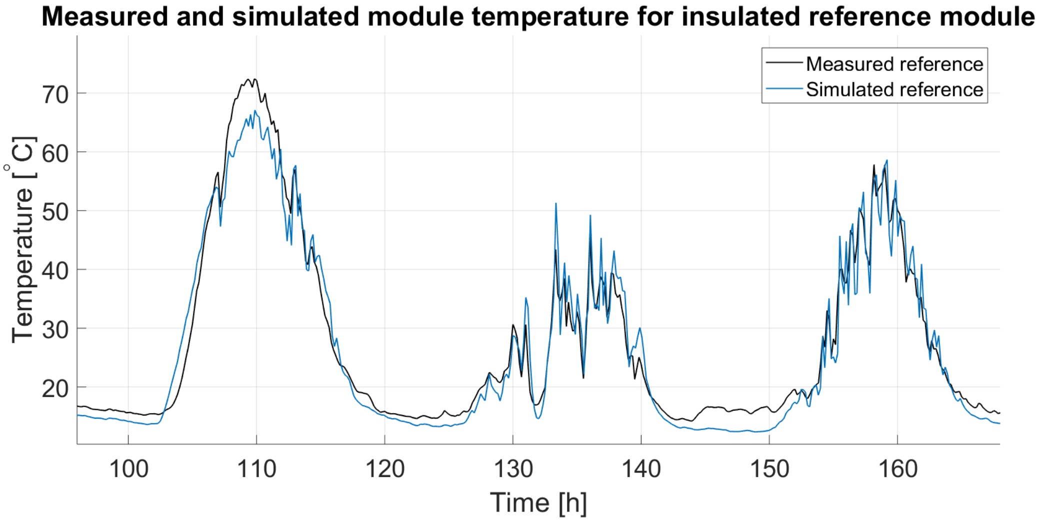

Figure 5.8: Measured and simulated module temperature for the reference module for three days of the measuring period.

On the contrary, when looking at the module temperature curve for the PCM module as presented in figure 5.9 it can be observed that during warm days the simulated curve follows the measured curve accurately. But during the night, the underestimation is larger than for the reference panel and during colder days the model overestimates the temperature. A similar trend is found for the PCMT module, a figure of which can be found in appendix D. A cause of this difference could be that for the reference module the insulation layer is not pressed on to the back of the panel as much as for the PV-PCM modules, due to the PCM slabs adding more thickness and thus allowing less space for the insulation material to sag in the middle. This sagging leads to a small layer of air between the back of the module and the insulation, this layer is not taken into account during the simulations. Since the frame could not be removed entirely on short notice this compromise had to be made when installing the thermal insulation layer.

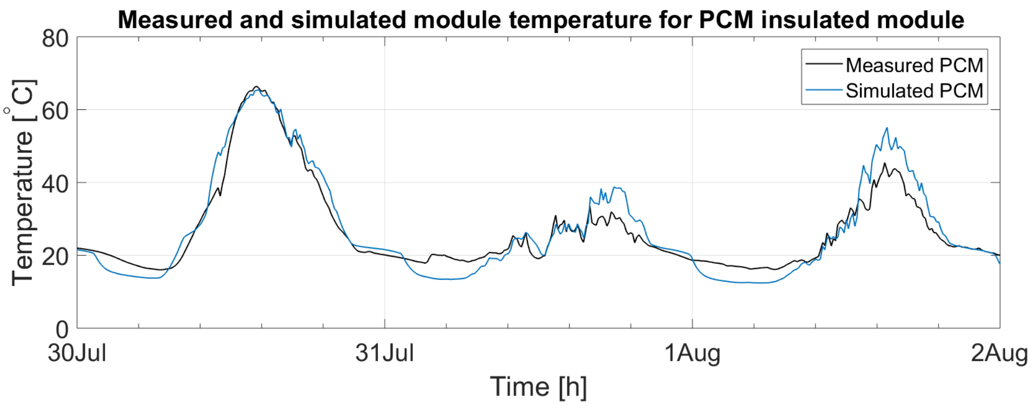

Figure 5.9: Measured and simulated module temperature for the PCM module for three days of the measuring period.

The RMSE values between measured data and simulated temperatures for the reference, PCM, and PCMT modules are 2.82$°C$, 3.74$°C$, and 3.11$°C$ respectively. The higher RMSE value for the PCM model is mostly due to the large underestimation of the module temperature during the night, which since there is little to no irradiance during these times, it will only have a small influence on the calculation of the effective temperature difference. The overall RMSE values are higher than in the previous model, therefore the predictions will be less accurate.

5.2.3. Predictions

Predictions for the optimal PCM parameters are again made using the Arici convection model, however the PVPortal data is not used as the way the data is created by averaging is found to be insufficiently accurate for the purpose of this research. Therefore, only the measured and PVGIS dataset are looked at. Since the peak module temperatures are higher for the insulated panels, it is expected that the optimum is at a higher temperature so simulations are done for a melting temperature of $20-30°C$ with $1°C$ incremental steps. Again the optimisation is done for a thickness of $1-5cm$ with steps of $1cm$. The predictions with the best preformance are shown in table 5.5, it is observed that the two data sets predict a different optimal melting temperature. However, the difference is only $1°C$, which can easily becaused by the weather conditions being different or the error in the simulations. For the measured data set the best results were found at a PCM thickness of $5cm$ and a melting temperature of $27°C$, a higher temperature than for the model without insulation. Meaning that it makes significant difference in choice of melting temperature if the module is installed in a free standing rack or integrated in a building. When taking an efficiency drop of $0.40-0.65\%/°C$[25] a decrease of $8.58°C$ can lead to a relative efficiency increase of $3.4-5.6\%$. In figure5.10 several days of the simulated data

Table 5.5: Table with the predicted best PCM parameters for the PVGIS and measured data.

	PVGIS	**Measured**
$d_{pcm}, T_{melt}, \Delta T$	$5cm, 26°C, -6.79°C$	$5cm, 27°C, -8.58°C$

results are shown for the predicted best performing situation using the PVGIS data. It can be observed that a significant temperature difference can be managed and maintained during the day, at the end of the day however the temperature will be higher due to the PCM cooling down slower than the PV.

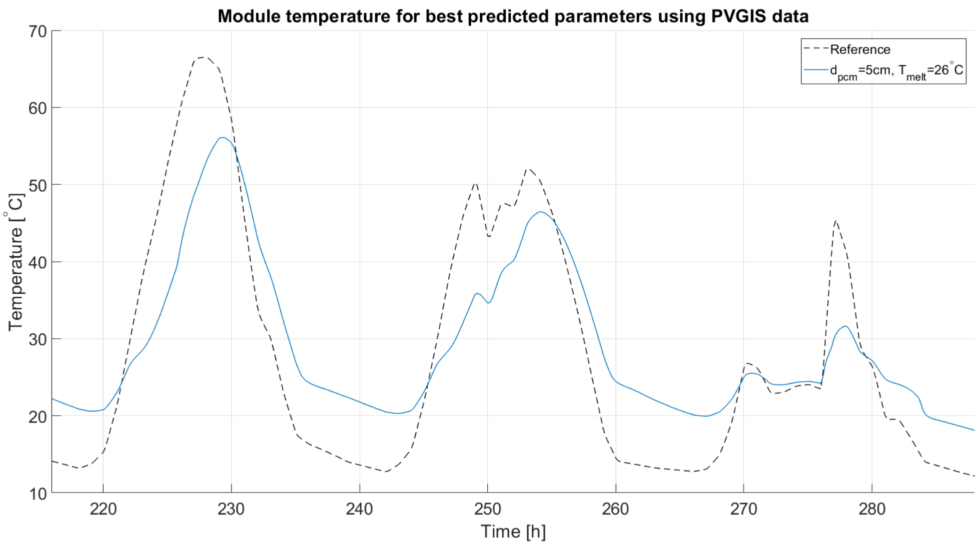

Figure 5.10: The predicted module temperature for the insulated simulation results of the PVGIS data of the situation with the best thermal performance.

Similarly, several days of the results using the measured data are presented in figure 5.11. A similar trend is observed the during the day a significant temperature reduction can be achieved. However, because of the larger fluctuations and the slower temperature response of the PV-PCM module it happens that during the temperature is higher than the reference module, for a short amount of time. This can be seen in figure 5.11 at 132 hours.

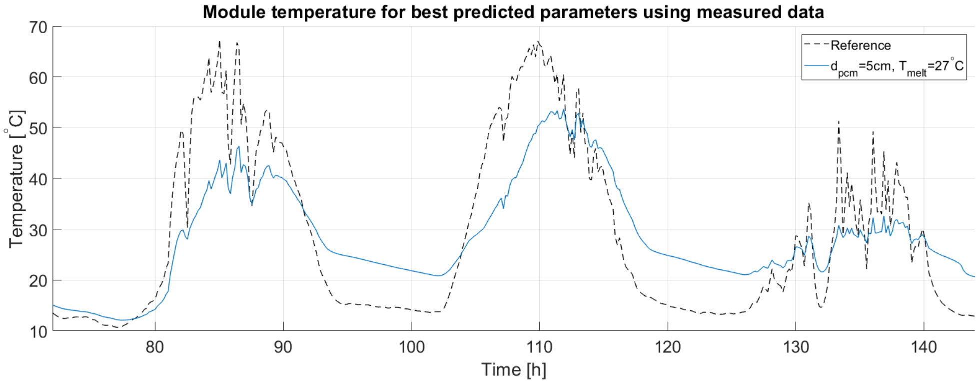

Figure 5.11: The predicted module temperature for the insulated simulation results of the measured data of the situation with the best thermal performance.

6 Conclusions & Recommendations

In this chapter the necessary conclusions are drawn and recommendations given for future research. This research has explored the viability of photovoltaic-phase change material (PV-PCM) system in both a free standing and emulated BIPV situation.

From simulations it was found that changing the parameters thickness and latent heat can have influence on the cooldown period of the PCM. Hence, increasing the thickness or latent heat raises the amount of heat that can be stored but also the storage time and as consequence it also takes longer to release the heat. Since, the latent heat is more difficult to control as it is a material property the thickness is an important variable to optimise the system for. Furthermore, the melting temperature has a large impact on the effectiveness of the cooling effect and is relatively simple to control, to an extend, by changing the chemical composition of the PCM slightly. The choice of the correct melting temperature is therefore important and depends highly on the climatic temperature and irradiance conditions.

Measurements were done in July 2019 in Delft on three different modules: a simple PV module to be used as reference, a module with a PCM slab attached at the back, and a module with a PCM slab that has a thermal paste between PV and PCM. It was found that the PCM actually had a negative effect on the module temperature, which was worsened by the thermal paste. Respectively the PCM and PCM+thermal paste (PCMT) modules had $0.52°C$ and $2.5°C$ higher effective temperature, the reason for this was found to be that the convective cooling effect was larger than the cooling provided by the PCM. The capacity for heat storage of the PCM was found to be too small, therefore it was functioning as an insulator hindering the convective cooling, this effect was only strengthened by the addition of the thermal paste layer which instead of improving the heat transfer to the PCM just acted as an additional thermal resistance.

The energy produced during the period of measurement was found to be 5.037, 5.093, $5.040kWh$ for the reference, PCM, and PCMT modules respectively. However since the difference is only around 1%, it was found to be uncertain if this increase in energy yield was caused by cooling effects.

A thermal model was created using *Comsol Multiphysics* and validated, afterwhich it was used to predict if a decrease in module temperature can be realised for this setup. From optimising the melting temperature and PCM thickness it was found that for a melting temperature of $23°C$ and $5cm$ of PCM the best results are obtained with an effective module temperature decrease of $-2.13°C$ can be achieved. The optimal parameters were used for simulation in a winter month (January) showing no adverse effects on module temperature.

Because convective cooling was having such a large effect on the module temperature and on of the goals was to test if a PV-PCM system would be useful for BIPV situations thermal insulation was installed behind each module. This insulation eliminates most of the convection and thereby a more accurate representation of a BIPV system is realised. Measurements were performed from the 26^{th} of July until the 7^{th} of August in 2019, with the same modules after installing *Armaflex* insulation material on the back side. The module temperature differences compared to the reference module were found to be $-6.69°C$ and $-5.09°C$ for the PCM and PCMT panels respectively. This resulted in an improvement in energy yield compared to the reference of 2.8% for the PCM panel and 1.4% for the PCMT panel. Moreover, the peak temperature difference that was measured in this period was $-21.7°C$. Showing that in fact for a setup close to BIPV conditions significant temperature reduction can be achieved.

Predictions were made for both the PVGIS dataset and the measured weather data again using the thermal model. Here it was found that the optimal thickness was $5cm$ and the optimal melting temperatures $26°C$

and 27°C for the PVGIS and measured data, respectively. Due to insulation the module temperature reaches higher values than before which causes the optimal melting temperature to be higher as well. It was predicted that the effective temperature differences reached for the PCM module are $-8.58°C$ for the measured data and $-6.79°C$ for the PVGIS data.

The most imporant conclusion that can be made from this research is that the wind speed plays a large role in the cooling of the modules. Therefore, PCM thermal management in free standing rack setups is not advisable especially in windy countries such as the Netherlands. Nevertheless, for BIPV situations where there is no wind behind the panels PCM cooling can achieve great results in reducing the module temperature during the day. Additionally, in BIPV situation the heat stored in the PCM can potentially be used in for thermal management of the building itself.

In future research in this topic the potential of PCM for building heating can be looked into, specifically the ease of heat extraction and the usefulness of the heat for other application. What definitely deserves more investigation is to integrate a PV-PCM system into an actual (piece of) wall to see if the results obtained in this research by eliminating convection on the rear side will also be seen in a more accurately represented building façade.

A
Effective temperature difference

In this appendix the method of calculating the effective temperature difference is explained. The difference in temperature cannot be compared one by one, because the absolute temperature difference has a more significant effect on the performance of the module with higher irradiance. Therefore, it is a weight is added to each temperature difference according to the irradiance value at that time normalised over the total irradiance received in the time span, as is shown in equation A.1. Here, $W(t)$ is the weight matrix and $G(t)$ is the irradiance.

$$W(t) = \frac{G(t)}{\Sigma_{t=0}^{t} G(t)} \tag{A.1}$$

This weight matrix is then multiplied with the temperature difference between the PCM module and the reference module, after which it is summed over the chosen time span, see equation A.2. This gives an weighted average temperature difference over the chosen time span.

$$\Delta T_{weighted} = \Sigma_{t=0}^{t} W(t) \left(T_{PCM}(t) - T_{ref}(t) \right) \tag{A.2}$$

B
Plane of Array Irradiance

This appendix describes the calculation of the plane of array (POA) irradiance from the Global Horizontal Irradiance (GHI), Direct Normal Irradiance (DNI), and Diffuse Horizontal Irradiance (DHI) using the location and the position of the sun. All factors are schematically shown in figure B.1.

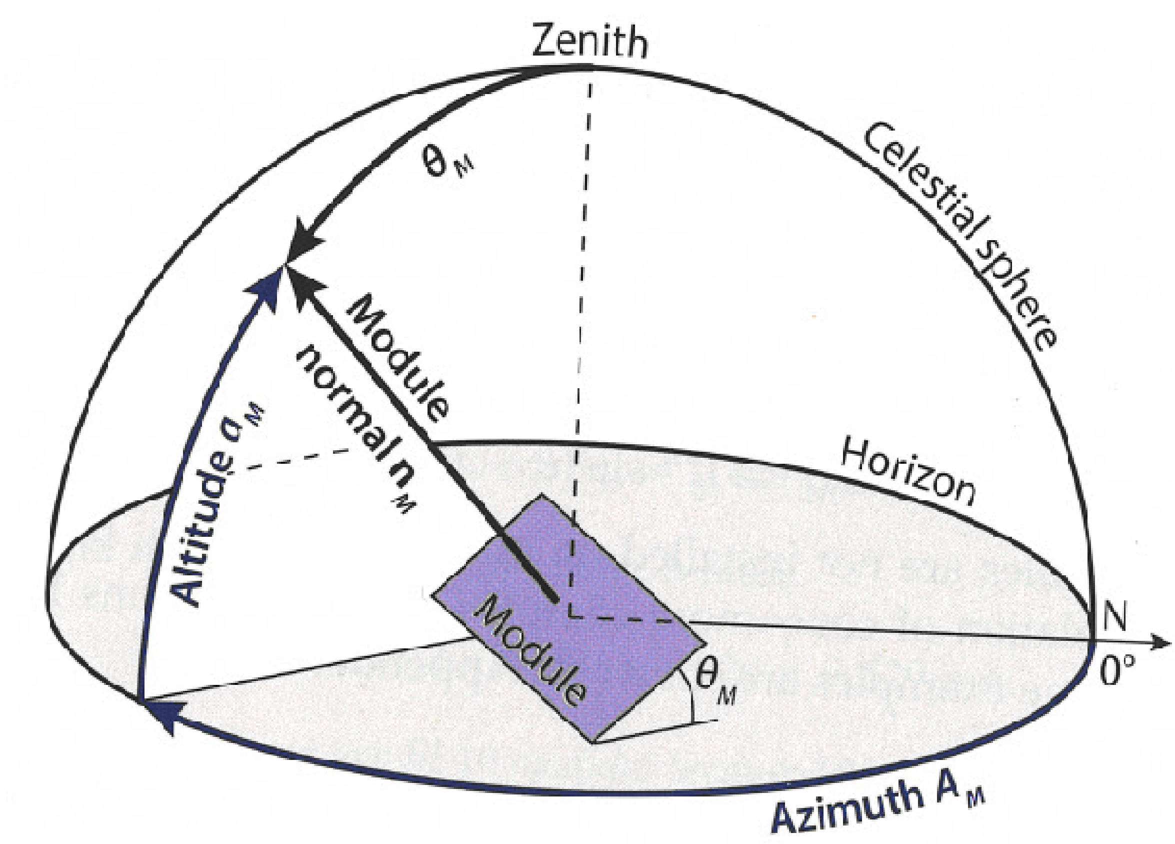

Figure B.1: Illustrating the angles used to describe the orientation of a PV module installed on a horizontal plane [9].

Starting with the direct plane of array irradiance, G_M^{dir}, given by equation B.1 here $cos\gamma$ is the cosine of the angle between the surface normal and the incident direction of the sunlight [9].

$$G_M^{dir} = DNIcos\gamma \tag{B.1}$$

$$cos\gamma = cosa_M cosa_s cos(A_M - A_s) + sina_M sina_s \tag{B.2}$$

The diffuse POA irradiance is given by equation B.3, where θ_M is the module angle of tilt.

$$G_M^{dif} = DHI\frac{1 + cos(\theta_M)}{2} \tag{B.3}$$

Reflected light from the ground also has a component depending on the albedo, a measure for the reflected light received from surroundings, is given by equation B.4. Here α is the albedo of the surroundings, for urban areas it is generally somewhere between 0.05 and 0.20 [9].

$$G_M^{gnd} = GHI\alpha\frac{1 - cos(\theta_M)}{2} \tag{B.4}$$

All these components can be added together as in equation B.5 leading to an estimate of the incident irradiance in the plane of array

$$G_M = G_M^{dir} + G_M^{dif} + G_M^{gnd} \tag{B.5}$$

C

Root mean square error

In this appendix the equation for the root mean square error (RMSE) is given in equation C.1, the RMSE gives the error between the simulated values and the observed values. Thereby, it gives a measure of accuracy, a smaller RMSE means more accurate predictions.

$$RMSE = \sqrt{\frac{\Sigma_{t=0}^{t}\left(T_{ref} - T_{PCM}\right)^2}{t}} \tag{C.1}$$

D
Validation Data

In this appendix the graphs of the comparison between measured and simulated data is presented for the whole measurement period.

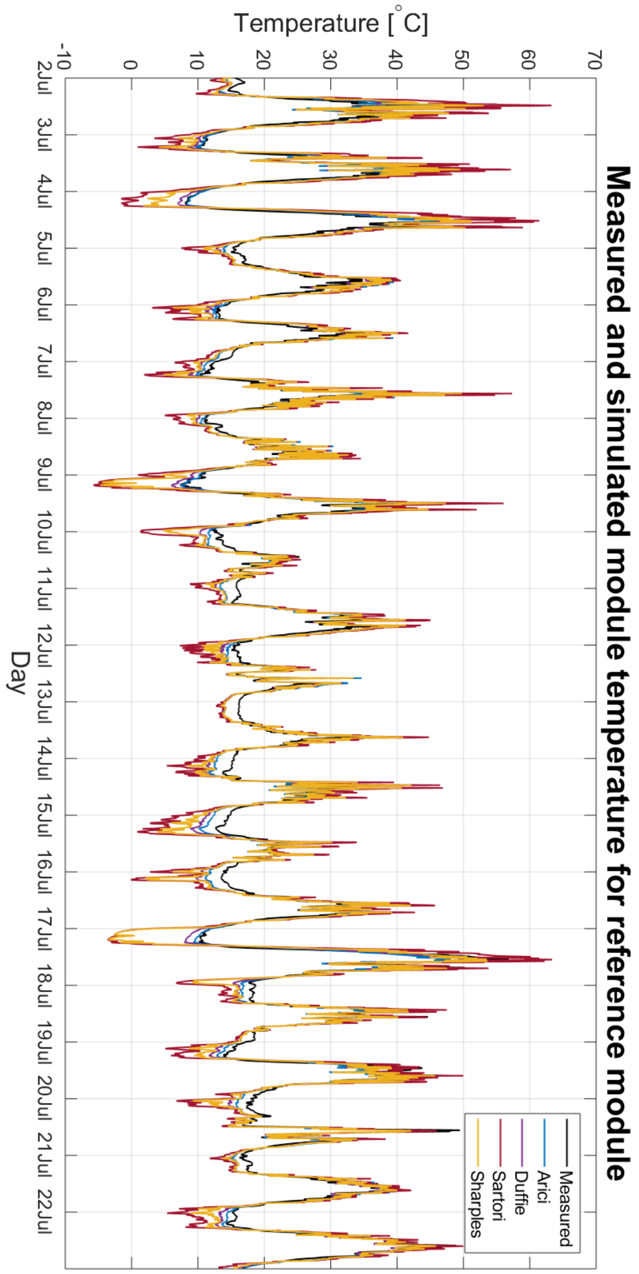

Figure D.1: Comparison of the measured and simulated data from 2-22 July.

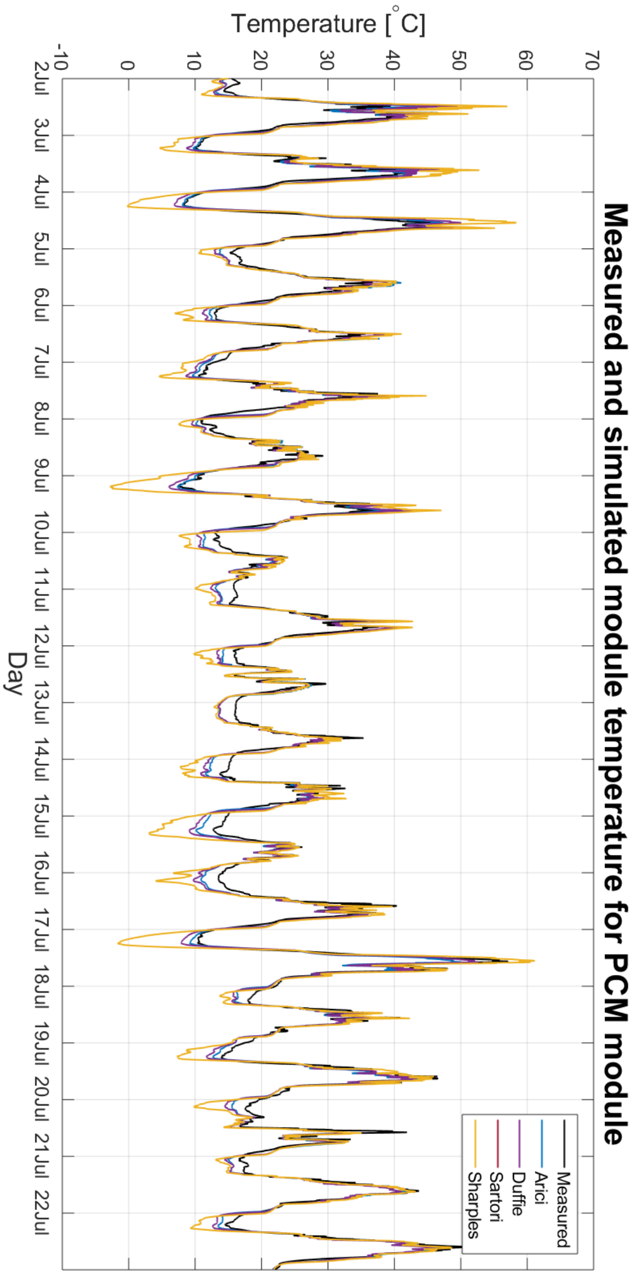

Figure D.2: Comparison of the measured and simulated data from 2-22 July for the PCM module.

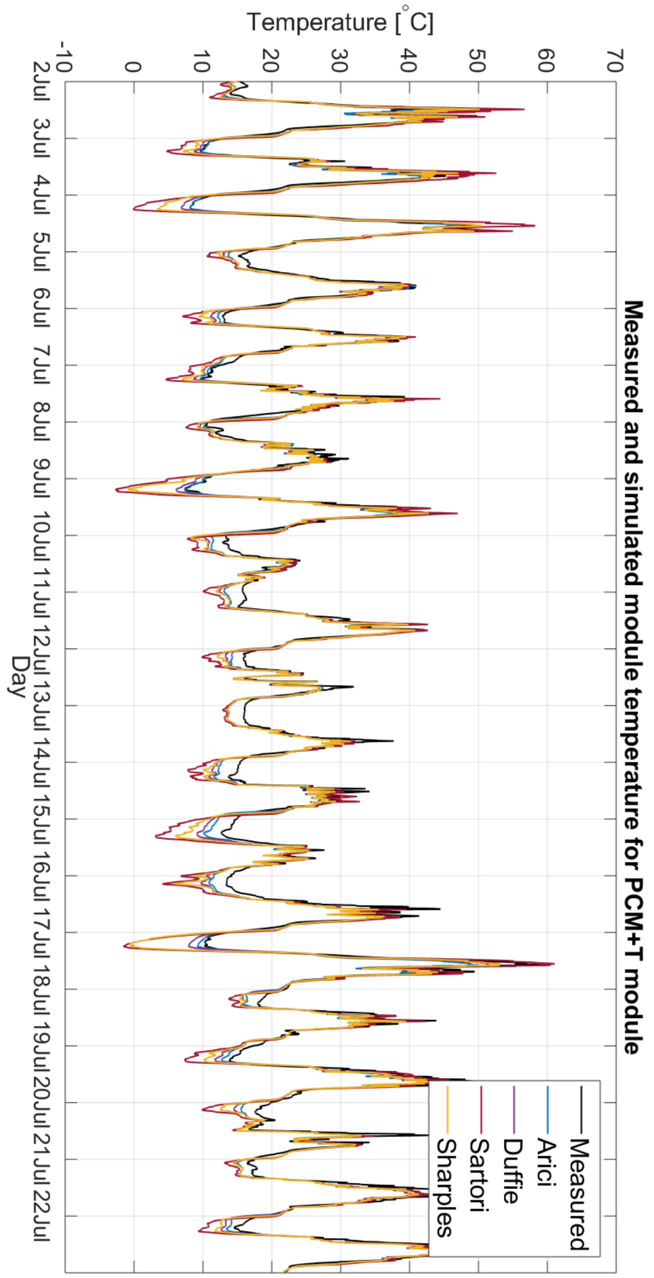

Figure D.3: Comparison of the measured and simulated data from 2-22 July for the PCM+T module.

Bibliography

[1] OC Autarkis. Pcm uitgelegd, 2019. URL `https://www.orangeclimate.com/nl/ocautarkis/producten/werking`.

[2] BloombergNEF. Cost of solar panels, 2016. URL `http://www.costofsolar.com/cost-of-solar-panels-10-charts-tell-you-everything/`.

[3] European Commission. Photovoltaic geographical information system, 2017. URL `https://re.jrc.ec.europa.eu/pvgis.html`.

[4] Comsol. The finite element method (fem), 2017. URL `https://www.comsol.com/multiphysics/finite-element-method`.

[5] Conrad. Conrad ctcm78-250 thermally conductive paste, 2019. URL `https://www.conrad.com/p/conrad-ctcm78-250-thermally-conductive-paste-78-wmk-525-g-max-temperature-150-c-1361504`.

[6] A. Hasan et al. Evaluation of phase change materials for thermal regulation enhancment of building integrated photovoltaics. *Solar Energy*, 84:1601–1612, 2010.

[7] A. Hasan et al. Yearly energy performance of photovoltaic-phase change material (pv-pcm) syste, in hot climate. *Solar Energy*, 146:417–429, 2017.

[8] A. Shukla et al. Cooling methodologies of photovoltaic module for enhancing electrical efficiency: A review. *Solar Energy Materials & Solar Cells*, 160:275–286, 2017.

[9] Arno Smets et al. *Solar Energy*. 2016.

[10] D. Otth et al. Assessing photovoltaic module degradation and lifetime from long term environmental tests. *Proceedings of the 1983 Institute of Environmental Sciences 29th Annual Meeting*, pages 121–126, 1983.

[11] J.A. Duffie et al. *Solar Engineering of Thermal Processes*. Wiley second edition, 1991.

[12] J.S. Stein et al. Measuring pv system series resistance without full iv curves. 2014.

[13] M. Araci et al. Phase change material based cooling of photovoltaic panel: A simplified numerical model for the optimization of the phase change material layer and general economic evaluation. *Journal of Cleaner Production*, 189:738–745, 2018.

[14] O. Dupré et al. Thermal behavior of photovoltaic devices: Physics and engineering. 2016.

[15] S. Sharples et al. Full scale measurements of wind-induced convective heat transfer from a roof mounted flat plate solar collector. *Solar Energy*, 62:69–78, 1998.

[16] Y. Jiang et al. Reduced operating temperature to improve durability and efficiency of solar modules. 2018.

[17] Ying-Ying Wu et al. Numerical study on convection heat transfer from inclined pv panel under windy environment. *Solar Energy*, 149:1–12, 2017.

[18] Walter Frei. Thermal modeling of phase-change materials with hysteresis, 2014. URL `https://www.comsol.com/blogs/thermal-modeling-of-phase-change-materials-with-hysteresis/`.

[19] Christiana Honsberg and Stuart Bowden. Series resistance, 2019. URL `https://www.pveducation.org/pvcdrom/solar-cell-operation/series-resistance`.

[20] William D. Callister Jr. *Materials Science and Engineering: An Introduction*. 1985.

[21] M. Keijzer. A multi-surface reflected irradiance model for pyranometer corrections and pv yield calculations in complex urban geometries. Master's thesis, Delft University of Technology, 2019.

[22] H. Mehlind and L.F. Cabeza. *Heat and Cold Storage with PCM: An Up to Date Introduction Into Basics and Applications.* Springer, 2008.

[23] A.F. Mills. *Basic Heat and Mass Transfer.* 2014.

[24] E. Radziemska. The effect of temperature on the power drop in crystalline silicon solar cells. *Renewable Energy*, 28:1–12, 2003.

[25] E. Radziemska and Klugmann. Thermally affected parameters of the current-voltage characteristics of silicon photocell. *Energy Conversion and Management*, 43:1889–1900, 2002.

[26] Ernani Sartori. Convection coefficient equations for forced air flow over flat surfaces. *Solar Energy*, 80: 1063–1071, 2005.

[27] Veikko Schepel. Dutch pv portal 2.0, 2019. URL `https://pvportal-2.ewi.tudelft.nl/MySQL/DownloadMap.php`.

[28] R. Stropnik and U. Stritih. Increasing the efficiency of pv panel with the use of pcm. *Renewable Energy*, 97:671–679, 2016.

[29] C. van Nierop y Sanchez. Phase change materials for thermal management of pv modules. Master's thesis, Delft University of Technology, 2019.

[30] B. Van Zeghbroeck. *Principles of Semiconductor Devices.* 1996.